Journal of Hydrology: Regional Studies 59 (2025) 102380

Contents lists available at ScienceDirect

Journal of Hydrology: Regional Studies

journal homepage: www.elsevier.com/locate/ejrh

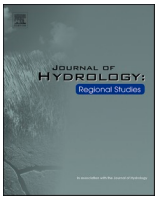

A comprehensive evaluation of the accuracy of satellite-based precipitation estimates over Thailand

Chanphit Kaprom [a], James Alexander Williams [a,c], Rajeshwar Mehrotra [b], Chainarong Ophaphaibun [a], Nutchanart Sriwongsitanon [a,*]

[a] *Remote Sensing Research Centre for Water Resources Management (SENSWAT), Department of Water Resources Engineering, Faculty of Engineering, Kasetsart University, Bangkok 10900, Thailand*
[b] *UNSW Water Research Centre, Vallentine Annexe (H22), Level 1, Room VA138, Kensington Campus, Sydney, NSW 2052, Australia*
[c] *GRC Hydro Pty Ltd, Level 20/66 Goulburn St, Sydney, NSW 2000, Australia*

ARTICLE INFO

Keywords:
Satellite-based Precipitation Estimate (SPE)
Bias Correction
Pixel-to-Point and Pixel-to-Pixel Comparisons
Accuracy based on rainfall probability and elevation
Ensemble Product
Thailand

ABSTRACT

Study region: Thailand
Study focus: This study assessed the performance of fifteen SPE products from the TRMM, GPM IMERG, CHIRP, CMORPH, and PERSIANN families, using 1779 gauged rainfall measurements, covering the period from 2001 to 2015, after undergoing fourteen quality control steps. Various statistical indicators ranked fifteen candidates with normalized scores, revealing performance differences across regions and products. This analysis helps to identify the most suitable products for specific objectives. It also evaluates the performance of SPEs across changes in elevation, rainfall probability, and data-scarce conditions by progressively reducing the amount of gauged rainfall data used. Finally, an ensemble product was developed.
New hydrological insights for the region under study: Firstly, CMORPH-BLD, CHIRPS-Preliminary, TRMM-3B42, and GPM IMERG-Final are the top four performers. Secondly, rainfall estimates from the SPE products were generally underestimated at rare probabilities and overestimated at more frequent ones. Their accuracy was slightly lower at elevations below 200 m, improved up to 800 m with consistent accuracy, and then decreased above 800 m, with minimal gauged rainfall stations increasing uncertainties in assessing SPE product performance at higher elevations. Thirdly, bias correction improved the performance of all SPEs, and accuracy gains were still achievable even with reduced gauged rainfall data. The ensemble of multiple SPEs reduced individual errors, demonstrating their reliability in representing precipitation in Thailand. These findings confirm the robustness of fixed simulation weights for future applications.

1. Introduction

Accurate information about precipitation, in time and space, is essential in numerous applications, including detection and prediction of flood (Tran et al., 2023) and droughts (Nguyen et al., 2024), studying climate trends (Lakshmi et al., 2024), hydrological

* Correspondence to: Remote Sensing Research Centre for Water Resources Management (SENSWAT), Department of Water Resources Engineering, Faculty of Engineering, Kasetsart University, 50 Phahonyothin Rd., Ladyao, Chatuchak, Bangkok 10900, Thailand.
E-mail addresses: chanphit.kap@ku.th (C. Kaprom), james@grchydro.com.au (J.A. Williams), raj.mehrotra@unsw.edu.au (R. Mehrotra), chainarong.opb@gmail.com (C. Ophaphaibun), fengnns@ku.ac.th (N. Sriwongsitanon).

https://doi.org/10.1016/j.ejrh.2025.102380
Received 31 August 2024; Received in revised form 10 March 2025; Accepted 6 April 2025

modelling (Tapas et al., 2024), crop water requirements (Pereira et al., 2021), and other water resources planning and management purposes in normal condition (Tapas et al., 2023; Nadeem et al., 2022; Gunathilake et al., 2020; Yang et al., 2020; Deng et al., 2018; Yuan et al., 2017; Duan and Bastiaanssen, 2013) and snow-based regions (Aryal et al., 2023). Traditionally, gauged rainfall networks are used to get this information (Le et al., 2023). However, the accuracy and availability of ground rainfall depends on the density and distribution of the observational network at a particular location (Gottardi et al., 2012). The observational network is primarily determined by site accessibility and the availability of resources (Skofronick-Jackson et al., 2017; Villarini et al., 2008). As a result, these networks are often sparse and unevenly distributed, particularly in mountainous and remote. This leads to inadequate representation of spatial patterns (Javanmard et al., 2010), leaving many areas, especially in developing countries, without sufficient coverage (Lakshmi et al., 2018; Mondal et al., 2018; Kidd et al., 2017; Rana et al., 2015). Studies indicate that the variability of precipitation in time and space plays a major role in introducing uncertainty in land surface hydrological simulations, significantly impacting modeling outcomes (Syed et al., 2004). Enhancing the accuracy of quantitative rainfall estimates is essential for effective flood risk management and addressing water resource challenges.

Alternative to gauged rainfall measurements is satellite-based precipitation estimate (SPE) products, which can effectively provide estimates of spatiotemporal variability of precipitation (Wen et al., 2021; Behrangi and Wen, 2017; Xie and Xiong, 2011). Originally, SPE products were developed using infrared (IR) information measured from geostationary satellites, microwave (MV) information from low earth orbiting satellites, or a combination of IR and MV (Kidd and Huffman, 2011). These so-called Satellite-based (S) precipitation products are renowned for their short latencies – but have limited accuracies due to inherent biases compared to gauged observations. As such, continuous development has been made over recent decades to improve accuracies. Satellite-gauge (SG) products (Funk et al., 2015; Huffman and Bolvin, 2013 and Huffman et al., 2007) are subsequently developed combined with rain gauged data (Xie and Xiong, 2011; Ebert et al., 2007). Some extensively used products include the TRMM Multisatellite Precipitation Analysis (TMPA) (Huffman et al., 2007), and Climate Prediction Center (CPC) Morphing (CMORPH) (Joyce et al., 2004), which both provide a spatial resolution of 0.25°. They are recognized as the best performing products in studies by Mondal et al. (2018); Simons et al. (2016); Li et al. (2015); Tan et al. (2015); Hu et al. (2014); Shen et al. (2010). In more recent SPE products, efforts to better capture the spatial variation of precipitation, as well as to provide longer temporal coverages to properly undertake performance evaluations have been introduced (Prakash et al., 2018; Yuan et al., 2018; Tan and Duan, 2017; Wang et al., 2017). This includes products such as the Integrated Multi-satellitE Retrievals for GPM (IMERG) (Huffman et al., 2015), Climate Hazards Group Infrared Precipitation with Stations (CHIRPS) (Funk et al., 2015), and Precipitation Estimation from Remotely Sensed Information using Artificial Neural Networks (PERSIANN) (Nguyen et al., 2018; Sorooshian et al., 2000). These products are shown to yield improved accuracies than pioneering products (Gunathilake et al., 2020; Poortinga et al., 2017; Duan et al., 2016; Pakoksung and Takagi, 2016).

Despite continual advancements in remote sensing, our knowledge of effective operation and use of the remote sensing data is still limited. For example, limitations of spectral, spatial and temporal resolution of satellite sensors, cloud cover mask, atmospheric conditions, and/or satellite unavailability for the required time and place. Gauged rainfall data is routinely used to validate and bias correct SPE products (Zhou et al., 2022; Gumindoga et al., 2019; Mastrantonas et al., 2019; Rasmy et al., 2014; Tian and Peters-Lidard, 2010). Furthermore, gauged rainfall data (point) is also used for performance evaluation and selection of SPE products (pixel). Pixel-to-point comparisons provide accuracy assessments at locations where gauged observations are available (Saemian et al., 2021; Tang et al., 2020). Furthermore, the interpolation of gauged observations onto grids permits comparison of gridded datasets (interpolated rainfall and gridded SPE) on the pixel-to-pixel. Duan et al. (2016) employed this approach to evaluate eight SPE products across different temporal scales (daily, monthly, and annual). Jiang et al. (2016) compared seven products at both daily and monthly scales, while Prakash (2019) focused on analyzing four SPE products exclusively at the monthly scale. When assessing the performance of SPE products over extensive regions, both pixel-to-point and pixel-to-pixel methods are useful for examining the effects of factors such as gauge density (Yu et al., 2020; Bai et al., 2019) and altitude (Jiang et al., 2016), which can influence the accuracy of different SPE products at local and/or broad scales.

The above forms the first objective of our study – the performance evaluations of fifteen SPE products across Thailand (over 500,000 km^2) using a dense gauged rainfall network over a period of fifteen years, through point-to-pixel and pixel-to-pixel comparisons. Given the study area is significant variability in elevation and rainfall frequency, the second objective is to assess how these factors influence the accuracy of the SPE products.

The availability of gauged rainfall data is pivotal for the successful validation and operational use of SPE products (Moges et al., 2022; Kumar et al., 2022; Tan et al., 2015; Tong et al., 2014). In regions with limited ground observations, it is important to determine what is adequate for reliable validation. With a readily available dense gauged rainfall network, the third objective of our study is to simulate scenarios with limited data by conducting a sensitivity test, progressively reducing the number of rain gauge stations to assess the impact on the accuracy of SPE products. The results of this analysis will significantly contribute to regions with limited gauged rainfall networks.

The performance of an individual SPE product at a given location is influenced by various factors, particularly the study area (Eini et al., 2022; Sun et al., 2018), the time of year (Tang et al., 2020b; Duan et al., 2016), and altitude (Derin et al., 2019; Guo et al., 2017). This forms the final objective of our study development of an ensemble product using all available SPE products over the country by pooling together all the available information and forming a weighted precipitation estimate for a given region and a given use.

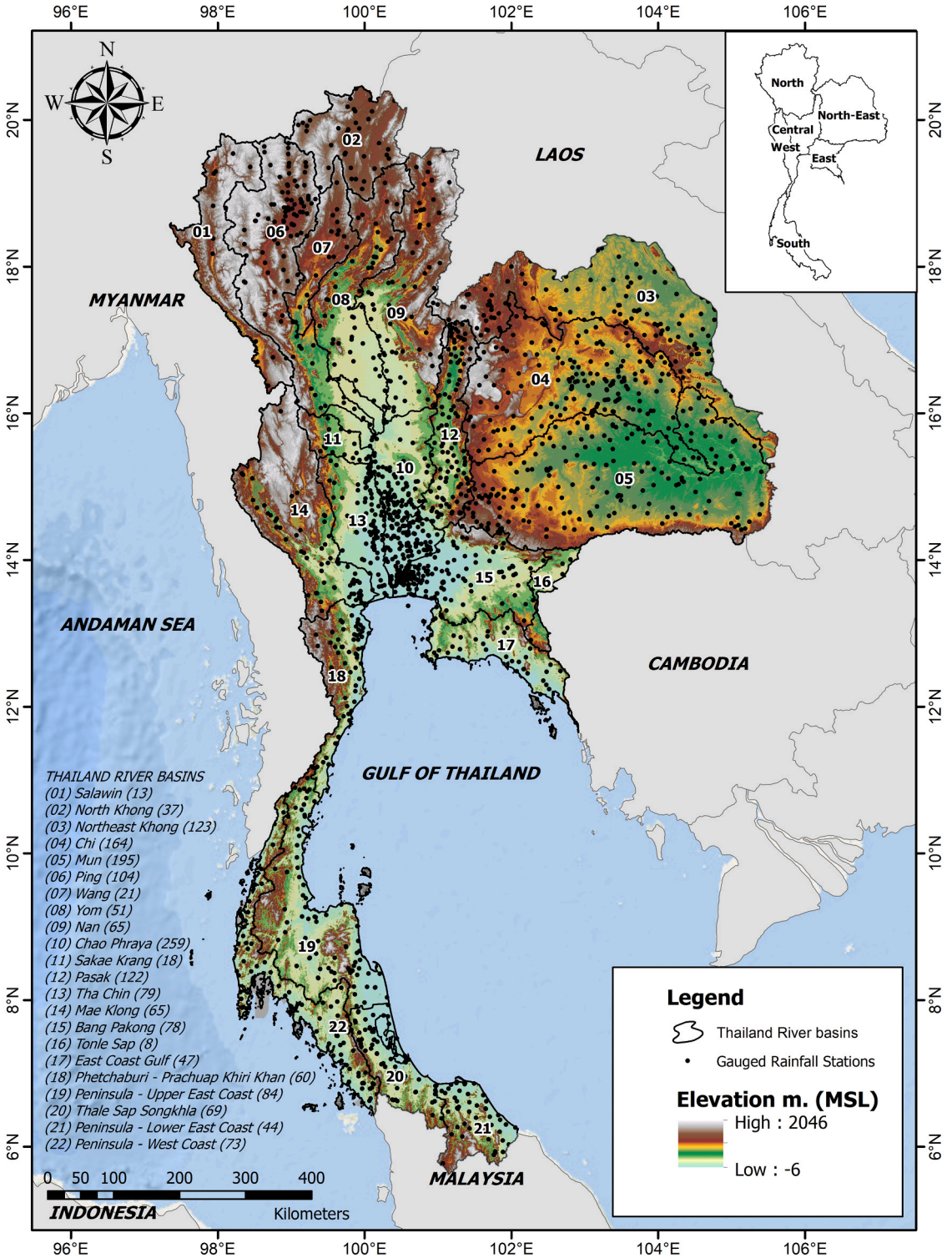

Fig. 1. Spatial distribution of 1779 gauged rainfall stations. Note: that the number of gauged rainfall stations in each sub-basin is shown in brackets.

2. Study area and data used

2.1. Study area

Thailand is situated between 97°22′E and 105°37′E, and between 5°37′N and 20°37′N. The country encompasses an area of 514,050 km^2, which is subdivided into 22 river basins. It is organized into six regions: North, Central, Northeast, East, West, and Southern, as shown in Fig. 1. The altitude ranges from −6–2046 m (MSL) and was derived using the SRTM-30 Digital Elevation Model (DEM) provided by the U.S. Geological Survey (USGS) (Mukul et al., 2015). The climate of Thailand is influenced by the Southwestern and Northeastern monsoons. The Southwestern monsoon brings moisture to the entire country between April and October. The Northeastern monsoon brings dry weather to mainland Thailand between November and March. However, Southern Thailand gets extra rainfall as moisture is picked up over the Gulf of Thailand. The estimated average annual rainfall of Thailand (from 2001 to 2015) is 1402 mm, while it is 2045 mm yr-1 over Southern Thailand (Sriwongsitanon et al., 2023). Fig. 1 also displays the spatial distribution of 1779 gauged rainfall stations used in the study. Most of these stations are in the Chao Phraya plain, which contains abundant rice fields. Since almost 90 % of rainfall occurs during the wet season, there is usually water shortage during the dry season (except for Southern Thailand), especially in river basins without medium- or large-scaled artificial water storages.

2.2. Data

2.2.1. Gauged rainfall data

The Thailand Meteorological Department (TMD) and Royal Irrigation Department (RID) are responsible for measuring rainfall. The TMD operates 1150 gauged rainfall stations. The RID has a special interest in micro-meteorological conditions over irrigated areas and operates 582 gauged rainfall stations. Some minor departments also operate 47 gauged rainfall stations for their specific purposes. All this information was pooled together and a total of 1779 gauged rainfall stations with temporal coverage from 2001 to 2015 were utilised in this study

2.2.2. Satellite-based precipitation estimate (SPE)

In total, fifteen SPE products are utilised in this study. These are categorized into two groups: satellite-based precipitation products (S) and satellite-gauge precipitation products (SG). Table 1 summarises the temporal and spatial resolutions, latency, available periods, and spatial coverage of the SPE products used in the study. These fifteen products belong to five families as discussed next.

Table 1
Descriptions of the satellite precipitation estimate (SPE) products used in this study.

SPE product		Abbreviation	Temporal Resolution	Latency	Temporal Period	Spatial Resolution	Spatial Coverage
Satellite-based precipitation (S) product	CHIRP-V2.0	CHIRP*	1 day	2 days	1981 – present	0.05°	50°S–50°N
	GPM IMERG-Early-V6	IMERG-E*	30 min	6 hours	2000 – present	0.10°	90°S–90°N
	GPM IMERG-Late-V6	IMERG-L*	30 min	18 hours	2000 – present	0.10°	90°S–90°N
	TRMM−3B42RT-V7	TR−3B42RT*	3 hours	8 hours	1998 – 2019	0.25°	50°S–50°N
	PERSIANN	PERSIANN*	1 hour	2 days	2000 – present	0.25°	60°S–60°N
	PERSIANN-CCS	P-CCS*	1 hour	1 hour	2003 – present	0.04°	60°S–60°N
	PERSAINN-PDIR	P-PDIR*	1 hour	15–60 mins	2000 – present	0.04°	60°S–60°N
Satellite-gauge precipitation (SG) product	CMORPH-BLD-V1.0	CM-BLD	1 day	2 months	1998 – present	0.25°	60°S–60°N
	CMORPH-CRT-V1.0	CM-CRT	1 day	2 months	1998 – present	0.25°	60°S–60°N
	CHIRPS-Preliminary-V1.8	CHIRP-PL	1 day	2 days	1981 – 2014	0.05°	50°S–50°N
	CHIRPS-V2.0	CHIRPS	1 day	3 weeks	1981 – present	0.05°	50°S–50°N
	GPM IMERG-Final-V6	IMERG-F	30 min	3.5 months	2000 – present	0.10°	90°S–90°N
	TRMM−3B42-V7	TR−3B42	3 hours	2 months	1998 – 2019	0.25°	50°S–50°N
	PERSIANN-CDR	P-CDR	1 day	3 months	1983 – present	0.25°	60°S–60°N
	PERSIANN-CCSCDR	P-CCSCDR	3 hours	3 months	1983 – present	0.04°	60°S–60°N

(1) TRMM Multi-satellite Precipitation Analysis (TMPA)

The Tropical Rainfall Measuring Mission (TRMM) Multi-satellite Precipitation Analysis (TMPA), developed by NASA, combines precipitation estimates from several satellites with gauged rainfall data (Huffman et al., 2007). The TMPA algorithm converts passive microwave (PM) fields of view from different sources and uses a C-band radar to determine the density of atmospheric water particles. Thermal infrared (IR) data from geosynchronous satellites provide cold cloud measurements that are merged into half-hourly $4 \times 4\ km^2$ gridded IR brightness temperature before being converted into IR precipitation estimates. TMPA precipitation data is available in near-real time (TRMM-3B42RT) and post-real time (TRMM-3B42) – the former being bias-corrected using monthly gauge rainfall data to generate the latter. The monthly rainfall estimates provided by TRMM-3B42 and TRMM-3B42RT were utilised in this study. The products can be downloaded from http://mirador.gsfc.nasa.gov.

(2) IMERG

After the retirement of TRMM satellite, NASA released the Integrated Multi-satellites for GPM (IMERG). The IMERG algorithm applies both infrared (IR) sensors and passive microwave (PMW) provided by the geostationary satellites and Low Earth Orbital (LEO), respectively. Although the inter-calibration process is identical to the TMPA algorithm, additional interpolation and re-calibration processes employ the Climate Prediction Center (CPC) morphing Kalman Filter technique and the Precipitation Estimation from Remotely Sensed Information using Artificial Neural Network-Cloud Classification System (PERSIANN-CCS), respectively. IMERG precipitation data are available in three products with different latencies: the two near-real-time products IMERG-Early and IMERG-Late with latencies of 6 hours and 18 hours, respectively and the final product using gauges rainfall data adjustment (IMERG-Final with a latency of 4 months). All three GPM IMERG-V06 products (GPM IMERG-Early, GPM IMERG-Late, and GPM IMERG-Final) were used in this study. These products have been retrospectively processed from the start of the TRMM era, which began in June 2000 and continues to the present. They were downloaded from https://gpm1.gesdisc.eosdis.nasa.gov/data/GPM_L3.

(3) CHIRPS

Funk et al. (2015) introduced the Climate Hazards Group Infrared Precipitation with Stations (CHIRPS), which supported effective hydrologic forecasts, agricultural drought monitoring and trend analyses in Southeastern Ethiopia. The dataset uses geostationary thermal infrared (IR) satellite observations to measure the Cold Cloud Duration (Milford et al., 1994), and yield pentadic IR estimates by regression against pentad estimates from TRMM-3B42V7 (Huffman et al., 2010; Huffman et al., 2007). By expressing the pentad IR estimates as a percentage of the long-term average, systematic bias is eliminated by multiplying the long-term average to the corresponding Climate Hazards Precipitation Climatology (CHPClim) pentad (Funk et al., 2012). The unbiased Climate Hazards Group Infrared Precipitation (CHIRP) dataset is blended to gauged rainfall stations to produce a rapid preliminary version (CHIRPS-Preliminary), and a later final version (CHIRPS). The CHIRPS-Preliminary uses the gauged rainfall stations belonging to Global Telecommunications System (GTS) and Conagua (Mexico). Its data is made available two days after the end of each pentad. Several other stations sources are used to generate the final version, available by the third week of the following month. These three products are used in this study and can be downloaded from http://chg.geog.ucsb.edu/data/chirps.

(4) CMORPH

The NOAA Climate Prediction Centre MORPHing method (CMORPH) estimates rainfall by combining rainfall estimates derived from passive microwave satellite observations and infrared data from geostationary satellites (Joyce et al., 2004). Infrared data is used to derive the cloud system advection vectors (CSAVs) to be later used to propagate passive microwave rainfall estimates in both forward and backward directions when passive microwave data is unavailable. Finally, the two propagated precipitation estimates are calculated using a time-weighted linear interpolation. Rainfall data provided by CMORPH's previous version (v0.x) were produced without applying either gauged rainfall data or a bias correction procedure. The latest version (v1.0) comprises three products: the raw SPE product (CMORPH-RAW); the bias corrected product (CMORPH-CRT) and the satellite-gauge blended product (CMORPH-BLD). Three spatial and temporal resolutions of CMORPH-RAW and CMORPH-CRT are available: including 8-km/30-min, 0.25°/3-hr, and 0.25°/daily. All three products are available at ftp://ftp.cpc.ncep.noaa.gov/precip/CMORPH_V1.0. Two products (CMORPH-CRT and CMORPH-BLD) were utilised in this study as they have the data available for the time period of interest.

(5) PERSIANN

The Precipitation Estimation from Remotely Sensed Information using Artificial Neural Networks (PERSIANN) was developed by The Center for Hydrometeorology and Remote Sensing (CHRS). The algorithm uses the Artificial Neural Networks (ANNs) to create the correlation between remotely sensed cloud-top temperature and the rain rate, which is provided by long-wave infrared (IR) sensor on GEO satellites and low Earth-orbiting satellites (LEO), respectively (Sorooshian et al., 2000; Hsu et al., 1997). The CHRS created two hydro-meteorological estimation algorithms: PERSIANN-Cloud Classification System (CCS) and PERSIANN-Climate Data Record (CDR). PERSIANN-CCS produces the near-real-time product with a higher spatial resolution than PERSIANN using a cloud clustering algorithm and IR data as the individual input. Meanwhile, the PERSIANN-CDR uses the PERSIANN algorithm with historical IR data since 1983. The CHRS Data Portal released the five PERSIANN-family products are comprised of the original PERSIANN, PERSIANN-CDR, PERSIANN-CCS, PDIR-Now, and PERSIANN-CCSCDR. The original PERSIANN product is more accurate than PERSIANN-CCS and more updated than PERSIANN-CDR. PERSIAN-CCS and PDIR-Now have the finest spatial resolution (0.04°) and provide real-time applications owing to a very short latency approximately of 15–60 mins. PERSIAN-CDR has the best accuracy as the monthly GPCP precipitation product was utilised to reduce biases. The PERSIANN-CCSCDR combines the algorithm between PERSIANN-CCS and PERSIANN-CDR and

leverages information from geostationary satellites to provide a fine spatiotemporal precipitation dataset with a long period of record. All PERSIANN-family precipitation datasets were utilised in this study and are downloaded from https://chrsdata.eng.uci.edu/.

3. Methodology

To achieve the objectives, the research methodology is divided into 5 steps, screening and processing of raw gauged rainfall data, performance evaluation, bias correction, sensitivity evaluation of the number of gauged rainfall stations and finally, the generation of an ensemble bias-corrected SPE product. These steps are summarized in Fig. 2 and discussed in detail next.

3.1. Screening and processing of raw gauged rainfall data

Gauged rainfall observations can be affected by errors from various sources, which may compromise their applicability in hydrological applications (Madsen, 1989). Therefore, it is essential to conduct a preliminary analysis to identify potential anomalies in the data (Reek et al., 1992; Abbott, 1986). This procedure is integral to the quality assurance of rainfall datasets, such as the Asian Precipitation Highly Resolved Observational Data Integration Towards Evaluation (APHRODITE) dataset (Yatagai et al., 2012) and has been applied in various studies (Jiang et al., 2023; Sharif et al., 2020; Tang et al., 2020a). In this study, we applied a quality control procedure proposed by Hamada et al. (2011) to screen the daily gauged rainfall dataset. The procedure consists of fourteen steps,

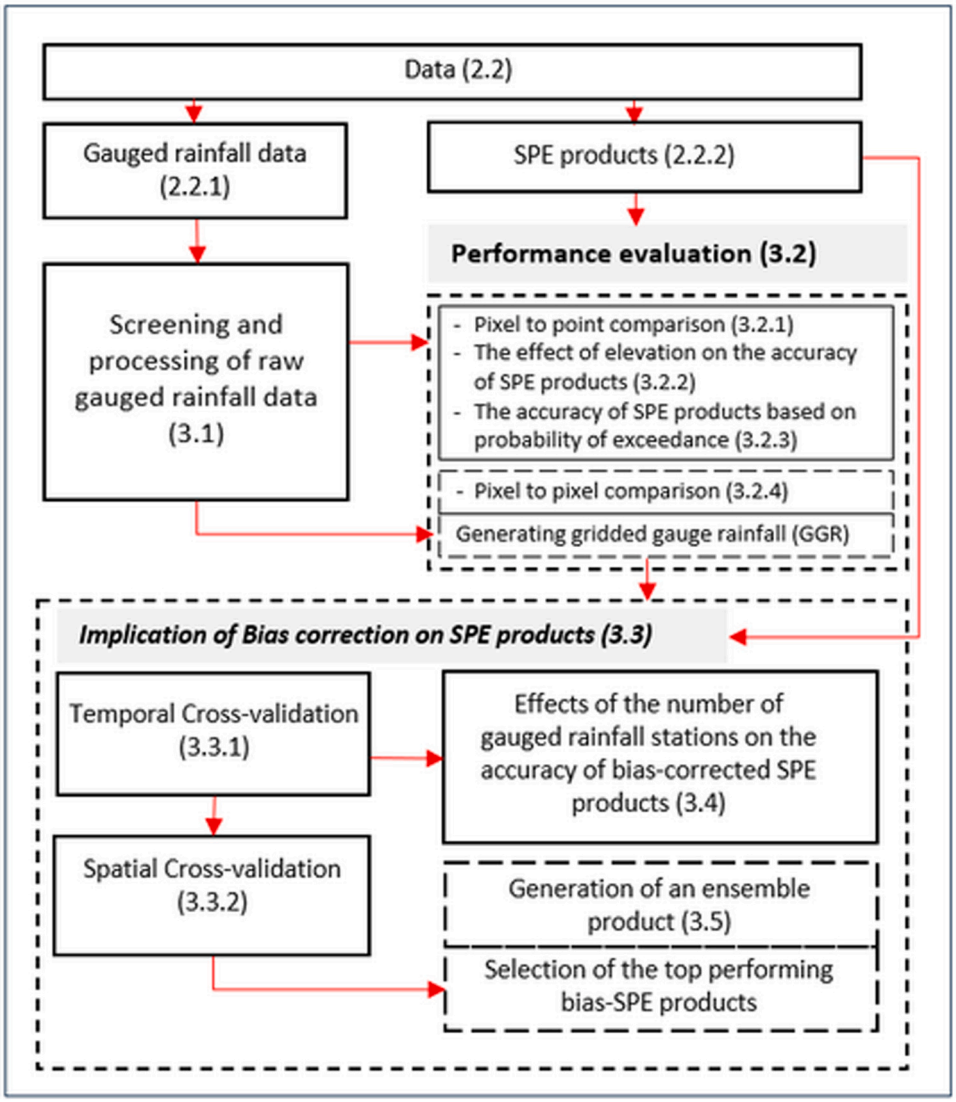

Fig. 2. Flowchart of methodology.

which can be grouped into three categories: metadata quality control, accuracy verification for each station's records, and reliability assessment across multiple stations. These categories are composed of 2, 10, and 2 steps, respectively. The full procedure, which includes all fourteen components designed to detect errors, is implemented in this study and detailed in Table S1 of the supplementary material.

Following the quality control procedure, the QC-checked daily series was aggregated to form monthly rainfall series (2001–2015) for further use in the research.

3.2. Performance Evaluation of raw SPE Products

The performance of raw SPE products is judged in two ways, pixel to point and pixel to pixel comparisons. The results are compared to assess the influence of interpolation of gauged rainfall data on the gridded data. The impact of elevation on the accuracy of SPE products, as well as their accuracy based on the probability of exceedance, is also evaluated and assessed. Four statistical indicators comprising Kling-Gupta efficiency (KGE) (Gupta et al., 2009), coefficient of determination (R^2) (Neter et al., 1996), mean bias error (MBE) (Willmott et al., 2005) and relative root mean square error (Rel. RMSE) (Moriasi et al., 2007) were calculated (see Table S2 of supplementary material for details). Taylor diagrams (Taylor, 2001) comprising the correlation coefficient (CC), standard deviation (STD) and the centred root mean square difference (RMSD) were also included and examined in the assessment.

3.2.1. Pixel-to-point comparison

The accuracy of SPE products was first assessed by pixel-to-point comparison to avoid possible errors caused by interpolation of gauged rainfall data to gridded data (Li et al., 2013). Monthly SPEs during the 2001–2015 period were extracted at the nearest locations of 1779 gauged rainfall stations and compared with the gauged rainfall.

3.2.2. The effect of elevation on the accuracy of SPE products

As discussed in Section 2.1, Thailand exhibits considerable variation in ground elevations. It would be of general interest to assess the impact of these variations on the accuracy of the SPE products. Therefore, the ground elevations at each gauged rainfall station location were recorded in the pixel-to-point comparison in Section 3.2.1. These elevations were then grouped into twelve intervals, each with a range of 100 m. The performance of the SPE products was ranked for each elevation interval, and an overall rank was derived across all intervals.

3.2.3. The accuracy of SPE products based on probability of exceedance

In general, SPE products have tendencies to underestimate retrievals of extreme rainfall (Jiang et al., 2018; Anjum et al., 2016; AghaKouchak et al., 2011) and overestimate retrievals of light rainfall (Liu et al., 2015). The efficacy for capturing the extreme values was evaluated by ranking the series and forming the exceedance probabilities of point gauged rainfall data and SPE products. The magnitude of bias in each SPE product was measured using the mean bias error (MBE).

3.2.4. Pixel-to-pixel comparison

Monthly gauged rainfall data were interpolated to generate gridded gauge rainfall (GGR) at a 0.01° grid scale. The data were then aggregated to larger grid scales of 0.04°, 0.05°, 0.10°, and 0.25° to match the grid cells of each SPE product, and the accuracy was assessed using KGE, R^2, MBE, and Rel. RMSE. The Inverse Distance Squared (IDS) method (Shepard, 1968), a widely used spatial interpolation technique, was applied in this study due to its reliability and efficient computation time (Maleika, 2020; Hu et al., 2014; Yong et al., 2010). This method has also been extensively used to generate gridded rainfall data for evaluating the performance of SPE products on a pixel-by-pixel basis (Sriwongsitanon et al., 2023; Duan et al., 2016; Jiang et al., 2016).

3.3. Implication of Bias correction on SPE products

Despite continual advancements in remote sensing, the SPE still have some limitations which limit their direct use in hydrological applications. These products require ground observations and adjustment methods to reduce systematic biases in the SPEs before their use in any study. Following it, we bias correct SPE products and evaluate their performance. Several simple and complex bias correction approaches are proposed in the literature. A few of them are selected and applied in the study as discussed next.

(1) Linear Bias Correction (LBC)

The linear bias correction (LBC) method has been applied to correct radar-based precipitation (Tesfagiorgis et al., 2011) and is also used to downscale global climate variables to a higher resolution in climate change studies (Lenderink et al., 2007; Teutschbein and Seibert, 2013). As the simplest bias correction approach, it has been used to bias-correct SPE products in many studies, including those by Gumindoga et al. (2019); Luo et al. (2018); Bhatti et al. (2016); and Habib et al. (2014). In this study, it was used as a baseline for comparison with other BC methods. A bias correction factor is derived for each pixel as the ratio of the GGR to the SPE datasets, summed over the entire time series, as expressed in Eq. (1).

$$SPE'_{(i)} = SPE_{(i)} \cdot \frac{\sum_{i=1}^{n} GGR_{(i)}}{\sum_{i=1}^{n} SPE_{(i)}} \quad (1)$$

where $SPE'_{(i)}$ is the bias-corrected SPE dataset of the i^{th} month, $SPE_{(i)}$ is the raw SPE dataset of the i^{th} month, $GGR_{(i)}$ is the GGR dataset of the i^{th} month, and n is the number of months.

(2) Bias correction using regression analysis (RABC)

Regression analysis has proven to be suitable for relating SPE products to gauged rainfall data (Deng et al., 2018; Al-Dousari et al., 2008; Omotosho and Oluwafemi, 2009). In this study, the second order polynomial as shown in Eq. (2) was selected to relate monthly GGR and SPE data. The bias correctors parameters a and b were then used to correct the raw SPE products. Here subscript i denotes *ith* month or time step of the series.

$$SPE'_{(i)} = aSPE^2_{(i)} + bSPE_{(i)} \tag{2}$$

(3) Bias correction using distribution transformation (DTBC)

This method transforms the distribution of the GGR data to match that of the SPE. This is achieved by performing Z-score normalization on the SPE data before fitting the mean and standard deviation of the GGR data. Chaudhary and Dhanya (2019) and Teutschbein and Seibert (2013) concluded that this method resulted in greater improvements in SPE products compared to the Quantile Mapping (QM) method. DTBC can be calculated using the following Eq. (3) (Bouwer et al., 2004).

$$SPE'_{(i)} = \left(\frac{SPE_{(i)} - SPE_{\mu}}{SPE_{\sigma}}\right) \times GGR_{\sigma} + GGR_{\mu} \tag{3}$$

where SPE_{μ} and SPE_{σ} are the mean and standard deviation of SPE dataset, GGR_{μ} and GGR_{σ} are the mean and standard deviation of the GGR dataset. The $SPE'_{(i)}$ and $SPE_{(i)}$ are the bias-corrected and raw SPE datasets for time step i, respectively.

(4) Quantiles mapping method (QM)

The initial assumption of applying the Quantile Mapping (QM) method is that the distributions of both GGR and SPE data can be well estimated by the gamma distribution, which was first used by Piani et al. (2010) for bias correcting precipitation in regional climate models. This method has been successfully applied for bias-correcting SPE estimates in various studies, including those by Ventura. (2020), Enayati et al. (2021), Luo et al. (2018), Yang et al. (2016), Cannon et al. (2015), Chen et al. (2013), Teutschbein and Seibert (2013), and Themeßl. (2011). The QM method has been shown to outperform simpler bias correction techniques, such as LBC and DTBC, in adjusting both the mean and variability of precipitation data (Chen et al., 2013; Teutschbein and Seibert, 2013; Gudmundsson et al., 2012). The probability density function (PDF) and cumulative distribution function (CDF) for GGR and SPE products are calculated using the Eqs. (4) and (5), respectively.

$$f(x) = \frac{1}{\beta^{\alpha}\tau(\alpha)} x^{\alpha-1}e^{-x/\beta} \tag{4}$$

$$F(x) = \int_0^x f(x)dx = \frac{1}{\beta^{\alpha}\tau(\alpha)} x^{\alpha-1}e^{-x/\beta} \tag{5}$$

$$SPE'(x) = F^{-1}(x) \tag{6}$$

where x is the GGR dataset, α and β, respectively, are the shape and scale parameters of the gamma distribution. These parameters are evaluated by the maximum likelihood estimation approach (Thom, 1966). The CDF of the SPE dataset was inversed by the transfer function (Eq. 6) using the parameters from the GGR dataset. QM can also be applied by considering an empirical distribution (Mehrotra and Sharma, 2016).

All Four BC procedures were examined in this study, each of which derive their bias correctors on a pixel basis. As the appropriateness of a BC procedure pertains to its usefulness in cross validation, two validation exercises were undertaken to test the robustness of all SPE products corrected by each of the BC procedures.

3.3.1. Temporal Cross Validation

Robustness in the temporal domain refers to the ability of a BC approach, calibrated using a part of the SPE rainfall, to assimilate left out SPE rainfall estimates (Sriwongsitanon et al., 2023; Siddig et al., 2022), with an accuracy similar to that produced using the data in calibration. For the sake of completeness, we adopted a leave-four years-out cross validation procedure here. GGR and SPE datasets were subdivided into sets of 11-year calibration and 4-year validation periods using a moving window of 4 years. The bias corrector(s) derived for each pixel in the calibration period were kept constant and used to validate the SPE dataset on the sliding 4 years 'testing window'. The bias-corrected SPE products were compared to the GGR dataset over the validation period to calculate the differences.

3.3.2. Spatial Cross Validation

Robustness in the spatial domain refers to the ability of a BC procedure to adequately assimilate SPE rainfall estimates for a given pixel using the bias correctors of the surrounding pixels (Cheema and Bastiaanssen, 2012). To test this, a leave out pixel process was performed by randomly dropping 30 % of the overall pixels. The bias corrector(s) of these left-out pixels were formed by the averaged

value(s) of the bias corrector(s) of their surrounding pixels. These estimated bias corrector(s) were applied to correct the raw SPE product and compared with the GGR dataset of those pixels. This procedure was repeated twenty times to ensure that whole region is covered and impartial results are obtained for each bias-corrected SPE product.

As pixels were randomly selected, there are chances that some of the pixels might be picked multiple times. This aspect was also investigated, and it was found that all pixels were selected at least once, and the duplication of pixels was also random.

3.4. Effects of the number of gauged rainfall stations on the accuracy of bias-corrected SPE products

The areal distribution of gauged rain stations is typically uneven, varying from one basin to another based on the region's importance, topography, and anthropogenic impacts. The average rainfall density is 378 km^2 per station. Rain gauge density ranges from 78.6 km^2 per station in the floodplain of the Chao Phraya basin, where Bangkok is located, to 1470 km^2 per station in the mountainous areas of the Salawin River basin. We investigated the effects of rain gauge station density on the bias-corrected (BC) results using the procedure outlined in Fig. 3. Only the best-performing BC method, as identified in Sections 3.3.1 and 3.3.2, was applied. Spatial cross-validation was performed by randomly excluding a fixed percentage of stations from each of the 22 sub-basins, then applying bias correction to the SPE products using the remaining stations. A total of ten scenarios were considered, starting from 90 %, 80 %, 70 %, 60 %, 50 %, 40 %, 30 %, 20 %, 10 %, and 5 % of the rainfall gauging stations, as detailed below.

Step 1: Perform BC on all SPE products using full network of gauge rainfall stations (GGR_{100}). Evaluate the performance of the bias-corrected SPE products against the GGR_{100} using the KGE indicator only.

Step 2: Incrementally reduce the density of gauged rainfall stations in each catchment area from 90 % to 5 % to produce the GGR datasets (i.e., GGR_{90}…, GGR_5) used to perform BC on all SPE products. To ensure the reliability of these results, randomly eliminate the gauged rainfall stations and repeat the procedure twenty times. Finally, calculate the performance of resultant bias-corrected SPE products as the averaged KGE across all iterations, and compare against GGR_{100}.

3.5. Generation of an ensemble bias-corrected SPE product

Recommending a particular SPE product for the study area might not help obtaining optimal results for all locations and seasons as the performance of an individual product might vary in time and space. The model averaging techniques produce a single piece of information from multiple ensemble members (SPEs), providing high accuracy (Muhammad et al., 2018; Beck et al., 2017; Poortinga et al., 2017). Therefore, with the availability of many SPE products, it makes sense to use an SPE product at a given location and time of the year which provides the best rainfall match. Keeping this in mind, as a final part of the research, the top four best-performing bias-corrected SPE products are pulled together to form a weighted data set at each grid point.

At a given location, the weights are allowed to vary with time and are formed based on the difference between bias-corrected SPE

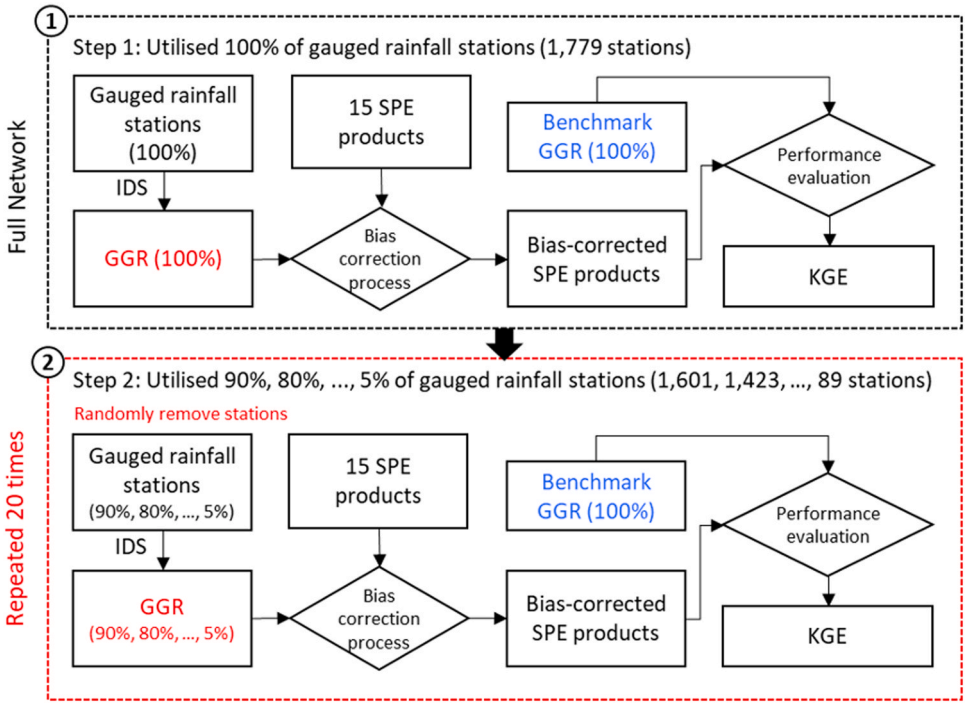

Fig. 3. A schematic of procedure adopted to study the variation of the density of gauged rainfall stations used in performing bias correction.

(BSPE) and GGR following Eq. (7). In this equation, n is the number of observations and m is the total number of SPE products, equals four here. W_i represents the weight of product *i*. The product with the minimum error is allocated maximum weight. These weights are then used to form the ensemble weighted average following Eq. (8).

$$W_i = \frac{\sum_{j=1}^{n} 1 \Big/ \left(BSPE_{j,i} - GGRj\right)^2}{\sum_{k=1}^{m} \sum_{j=1}^{n} 1 \Big/ \left(BSPE_{j,k} - GGRj\right)^2} \tag{7}$$

$$SPE_E = \sum_{i=1}^{m} W_i BSPE_i \tag{8}$$

To assess the robustness of the estimated weights, we again apply cross validation in time. Following the earlier procedure, 30 % of data is retained and the weights were estimated by using the remaining 70 % of data and Eq. (7). The estimated weights are used with the calibrated as well as retained 30 % of data to get the weighted time series for both time periods which was compared against the observed GGR_{100} to get the KGE values. These steps are summarized in Fig. 4

4. Results

4.1. Screening and processing of raw rainfall data

The outcome of quality control procedure is presented in Table S3 of supplementary material which summarises data-related inconsistencies detected by the QC procedures. In total, 46,829 (0.719 %) daily records were identified by the QC procedures as questionable. These were substituted by the records of nearby stations. The processed records were used in subsequent analyses.

4.2. Performance Evaluation of Raw SPE Products

The results of the raw SPE products are organized into four sections: first, the accuracy based on the pixel-to-point comparison; second and third, the impact of elevation and accuracy based on probability of exceedance; and finally, the accuracy based on the pixel-to-pixel comparison.

4.2.1. Pixel-to-point comparison

Overall, as expected, SG products provided better performance than S products (detailed results are shown by the first and second boxplots of each statistical indicator in Figure S1 of supplementary material). The performances of all SPE products, derived in terms of the median (p50) of the four indicators, is summarised in Table 2. The four performance indicators were scaled (between 0 and 1) and

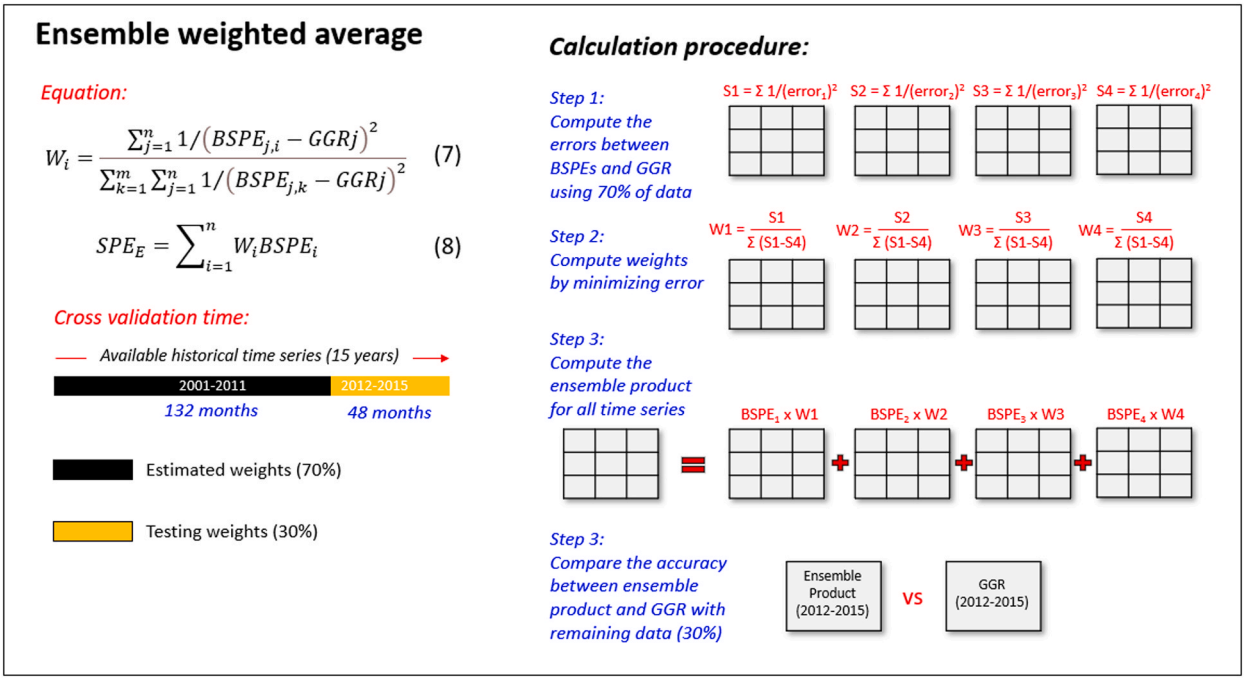

Fig. 4. Generation of an ensemble bias-corrected SPE product.

Table 2
Scaled scores of 15 SPE products based on all four statistical indicators.

SPE Products	KGE		MBE		Rel. RMSE		R^2		Average scaled score
	P_{50}	û	P_{50}	û	P_{50}	û	P_{50}	û	
CHIRPS-PL	0.71	0.96	-3.40	1.00	67.00	1.00	0.63	0.80	0.94
CM-BLD	0.72	0.99	6.70	0.78	67.30	0.99	0.66	0.92	0.92
TR-3B42	0.72	1.00	14.10	0.62	67.70	0.98	0.66	0.97	0.89
CM-CRT	0.71	0.96	4.80	0.82	69.80	0.93	0.63	0.75	0.87
IMERG-F	0.69	0.91	20.70	0.48	68.80	0.96	0.67	1.00	0.84
CHIRPS	0.69	0.91	17.30	0.55	71.70	0.89	0.64	0.83	0.79
CHIRP*	0.68	0.90	12.80	0.65	72.20	0.87	0.61	0.65	0.77
P-CDR	0.54	0.49	32.60	0.22	78.80	0.71	0.66	0.94	0.59
TR-3B42RT*	0.61	0.67	24.70	0.39	81.80	0.64	0.60	0.60	0.57
PERSIANN*	0.56	0.53	18.50	0.52	86.30	0.53	0.51	0.12	0.43
IMERG-L*	0.56	0.53	30.00	0.27	87.30	0.51	0.56	0.38	0.42
IMERG-E*	0.55	0.49	32.60	0.22	87.20	0.51	0.56	0.38	0.40
P-CCS*	0.48	0.29	29.50	0.28	95.30	0.31	0.54	0.26	0.29
P-CCSCDR	0.38	0.00	42.50	0.00	100.50	0.18	0.60	0.58	0.19
P-PDIR*	0.38	0.02	40.90	0.03	108.10	0.00	0.49	0.00	0.01
Average	**0.60**	**-**	**21.62**	**-**	**80.65**	**-**	**0.60**	**-**	**-**

Note: P_{50} is the median and **û** is the scaled score

averaged across to form a single score of overall performance. Results suggest that CHIRPS-Preliminary gained the highest score (0.94) followed by CMORPH-BLD (0.92), TRMM-3B42 (0.89), CMORPH-CRT (0.87), GPM IMERG-Final (0.84) and CHIRPS (0.79) which are all SG products. CHIRP (0.77), the only S product, performs marginally better than PERSIANN-CDR (0.59) and PERSIANN-CCSCDR (0.19), the SG product. Among S products, TRMM-3B42RT (0.57) provided better performance compared to PERSIANN (0.42), GPM IMERG-Late (0.42) and GPM IMERG-Early (0.40), respectively. PERSIANN-PDIR, PERSIANN-CCSCDR and PERSIANN-CCS, which are all PERSIANN products, attracted very low scores of 0.10, 0.19 and 0.29, respectively. These results highlight the benefits of incorporating rain gauge information in satellite-based rainfall retrieval algorithms.

The accuracy of SPE products was further assessed using Taylor diagrams (Taylor, 2001), which evaluates the performances of three statistical measures: the correlation coefficient (CC), standard deviation (STD) and the centered root mean square difference (RMSD) (equations are shown in Table S2 of the supplementary material). In addition to the monthly-scale comparisons, performances at seasonal and annual time scales were also investigated. In the Taylor diagrams (Figure S2 of supplementary material), the CC, STD and RMSD values of each product were averaged across 1779 gauged rainfall stations. Each product is represented as a point on the diagrams (circles for SG products and triangles for S products), whilst the red circle on the X-axis represents the observed value. Again, as anticipated, all SG products generally perform better (i.e., situated closer to the observed value) than the S products for all time scales. CC values at monthly scale (approx. 0.7–0.8) are generally higher than those of the dry season (approx. 0.5–0.6), wet season (approx. 0.4–0.5), and annual scale (approx. 0.3–0.5), respectively.

Further, to quantify the performances of each SPE product, a scaled score was devised. Here, the best performing SPE product (i.e., located closest to the observed point) receives a score of 1, while others being away, receive lower scores. The score is calculated as the ratio of the distance between each SPE product to the observed point and the distance between the best SPE product and the observed point. An average score was calculated as the average across the four timescales.

GPM IMERG-Final gained the highest average score of 1.0 and PERSIANN-PDIR attained the lowest average score of 0.62. All SG products received scores of above 0.94 – higher than all S products, except PERSIAN-CCSCDR gained a score of 0.77. CHIRP was ranked as the most reliable S product with the score of 0.91, while all PERSIANN S products were ranked as the three worst performers These scores are presented in the bottom table of Figure S2 of the supplementary material, for all timescales and SPE products.

The overall results of pixel-to-point comparison indicated the five best performing products, CMORPH-BLD, TRMM-3B42, CMORPH-CRT, GPM IMERG-Final and CHIRPS. The Taylor diagrams also picked the same top five products, but in a slightly different order: GPM IMERG-Final, CMORPH-BLD, TRMM-3B42, CMORPH-CRT and CHIRPS-Preliminary. This difference could pertain to the different statistical indicators used in the tests.

4.2.2. The effect of elevation on the accuracy of raw SPE products

Performance of SPE products was evaluated based on the altitude of the location of the corresponding gauge rainfall station. TRMM-3B42 was found to be the best performer, receiving an average rank of 2.3. This was followed by CMORPH-BLD (4.0), GPM IMERG-Final (4.6), CHIRPS (5.0), CHIRPS-Preliminary (5.8) and CHIRP (6.0). Meanwhile, PERSIANN products were among the worst performers. Overall, the accuracies are greatest in the 600–700 m elevation range but tails off at both lower and higher elevations. Figure S3 of supplementary material provides more details.

The figure shows the KGE values for the top five best-performing products across various elevation ranges: < 200 m, 200–400 m, 400–600 m, 600–800 m, 800–1000 m, and > 1000 m, with values of 0.62, 0.71, 0.71, 0.71, 0.68, and 0.54, respectively. The percentage of rainfall stations for each elevation band is 78.2 %, 15.0 %, 4.2 %, 1.5 %, 0.8 %, and 0.4 %, respectively. The SPE products showed relatively lower accuracies near sea level (0–200 m), with accuracy remaining consistent between elevations of 200–800 m. The high density of gauged rainfall stations at these lower elevations strengthens the reliability of the observed data and highlights the varying sensitivity of SPE products to these factors.

Accuracy begins to marginally decrease between 800 and 1000 m and continues to decline above 1000 m. However, the number of gauged rainfall stations in these two higher elevation bands is only 0.8 % and 0.4 % of the total stations, respectively. At higher elevations, uncertainties in gauged rainfall data may also arise due to the sparse station distribution, making it more difficult to assess the robust performance of the SPE products at these elevations.

4.2.3. *The accuracy of raw SPE products based on probability of exceedance*

Fig. 5a presents the average rainfall depths of observed data (1779 stations) across different probabilities of exceedance (Pr). This is overlayed with rainfall depths of SPE products at corresponding Pr. The figure demonstrates underestimated retrievals at rare Pr and overestimated retrievals of SPE products at more frequent Pr. Each product intercepts the plot of observed data at a probability, that defines the transition between under- and overestimation. Notably, the SPE products which best resemble the observed data at rarer Pr (e.g., PERSIANN-PDIR and PERSIANN-CCSCDR, intercept atPr = 12 % and 8 %, respectively) yield greatest error at more frequent Pr. On other hand, products such as PERSIANN and CHIRPS-Preliminary, which intercept atPr = 39 % and 47 %, respectively, best resemble the observed data at more frequent Pr, but greatly underestimate rainfall at rarer Pr.

Fig. 5b presents the accumulated errors (summation of absolute differences of GGR and SPE) due to both under- and overestimations over the 180-month study period, as presented in gray and pink bars in Fig. 5b, respectively. CHIRPS-Preliminary yielded the least total error (5036 mm), followed by CMORPH-CRT (5380 mm) and CMORPH-BLD (5584 mm). CHIRPS-Preliminary underestimates rainfall of Pr < 47 % by 2619 mm, and overestimating Pr > 47 % by 2418 mm. PERSIANN-CCSCDR (total error = 8799 mm) was most accurate for estimating rarer events, underestimating rainfall of Pr < 8 % by 365 mm, but grossly overestimates rainfall of Pr > 8 % by 8435 mm.

The results of this study showed that all fifteen SPE products exhibited significant biases during extreme monthly rainfall events. These findings are consistent with previous studies by Jiang et al. (2019), Huang et al. (2018), and Tan et al. (2015). However, the study also revealed that PERSIANN-PDIR and PERSIANN-CCSCDR demonstrated relatively lower errors for these rare events, indicating superior performance in detecting extreme monthly rainfall. These results are also in line with prior research by Baig et al. (2023) and Sadeghi et al. (2021).

4.2.4. *Pixel-to-pixel comparison*

Pixel-to-pixel accuracy comparison are presented at national and regional levels (Northern, Northeastern, Central, Eastern, Western and Southern Thailand). Fig. 6a presents the spatial variation of KGE (between monthly GGR and SPE data) over Thailand. The figure shows that CHIRPS-Preliminary stood as the top product (KGE = 0.75) and PERSIANN-CCSCDR ranked as the worst product

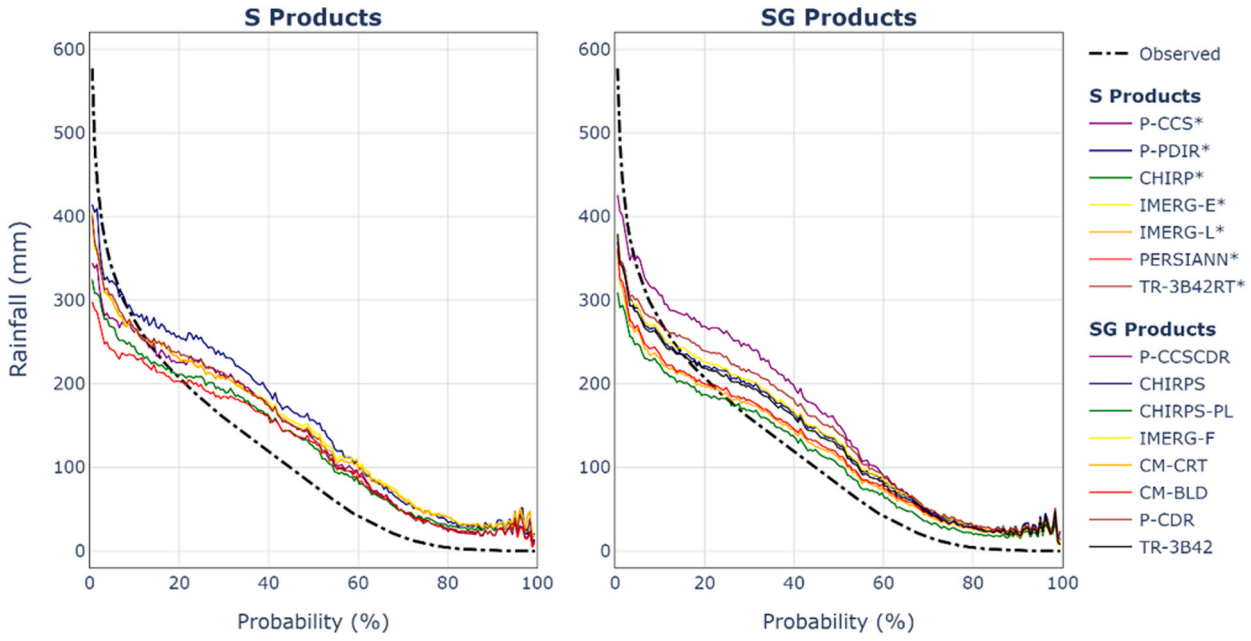

Fig. 5. **a** Average rainfall depths of gauged rainfall data (1779 stations) across different probabilities of exceedance (Pr) compared to SPE products.

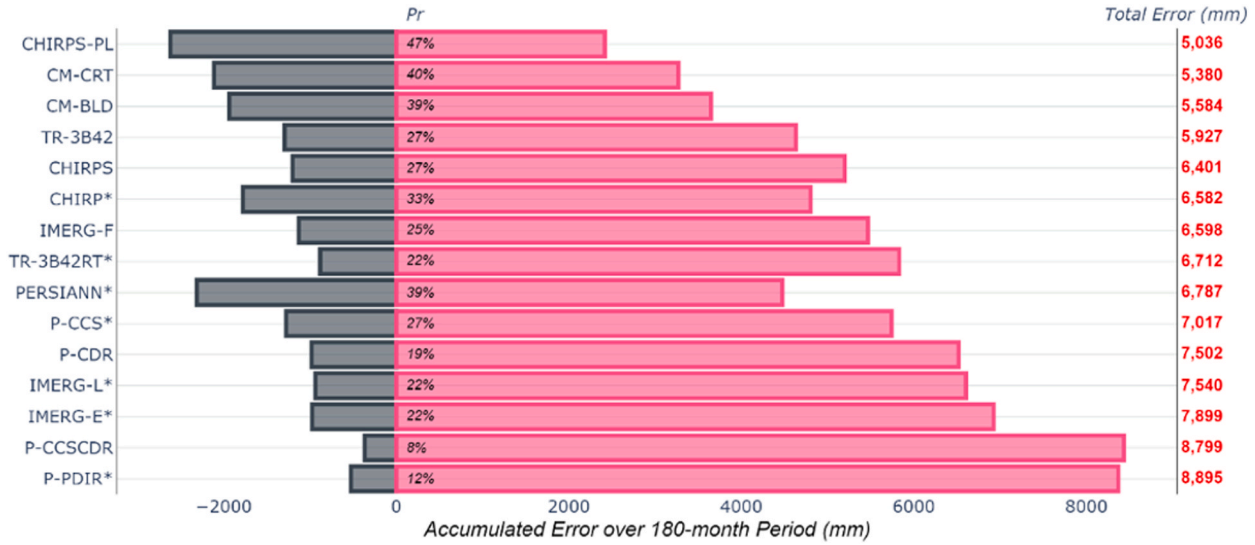

Fig. 5. b Accumulated error (absolute differences) of SPE products relative to gauged rainfall data. The gray and pink bars represent the accumulated errors from underestimations and overestimations, respectively, over the 180-month study period. **Note:** Grey bar represents underestimation; Pink bar represents overestimation.

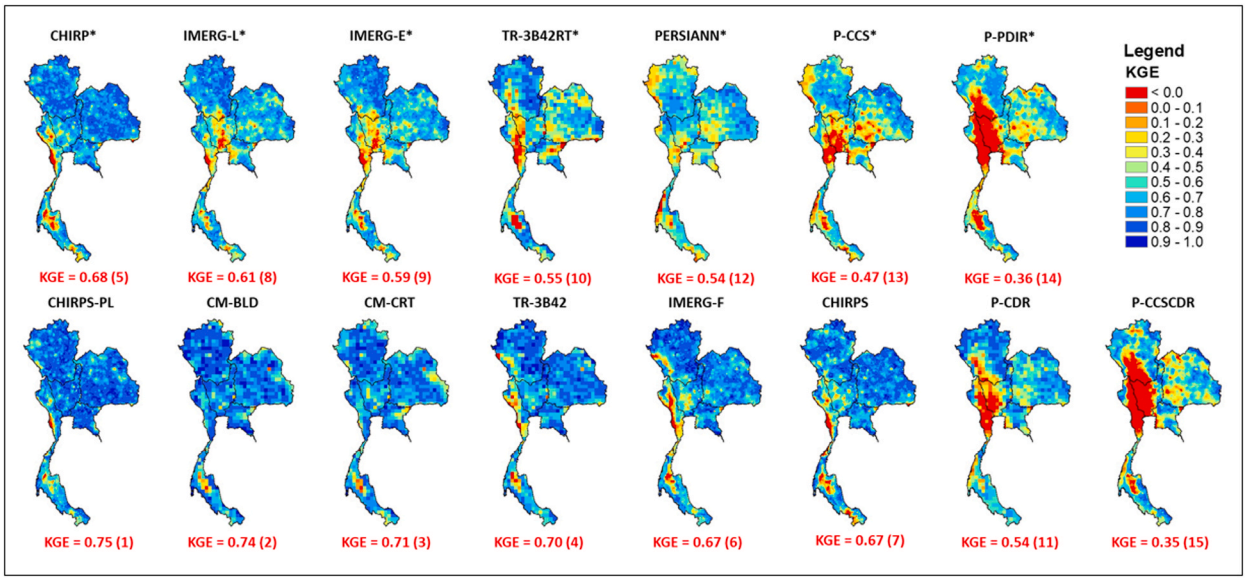

Fig. 6. a Spatial variation of KGE (of monthly GGR and SPE products). The values in brackets represent the performance ranking of SPE products.

(KGE = 0.35). All PERSIANN products are among the five worst performers, and they show low accuracy among the pixels located in Western, Southern, and Central Thailand.

Further, to explore the performances of the SPE products across the study area, the highest-ranked SPE product for each pixel was determined and presented in the second column of Fig. 6b. Among the S products, CHIRP is the best performer across 47.3 % of the total pixels, followed by TRMM-3B42RT, GPM IMERG-Late; PERSIANN; GPM IMERG-Early; PERSIANN-CCS and PERSIANN-PDIR, covering 18.8 %; 14.1 %; 10.0 %; 4.4 %; 4.3 %, and 1 % of the study area, respectively. For SG products, CHIRPS-Preliminary is the best performer across 29.6 % of the total pixels, followed by CMORPH-BLD; TRMM-3B42; CMORPH-CRT; CHIRPS; GPM IMERG-Final; PERSIANN-CDR and PERSIANN-CCSCDR, covering 23.7 %; 11.2 %; 10.9 %; 10.2 %; 8.5 %; 4.3 % and 1.7 % of the study area, respectively. At the regional level, CHIRP and CHIRPS-Preliminary are dominant in the Northeast (67.5 % and 35.1 %), Central (57.6 % and 58.4 %) and East (64.7 % and 44.1 %). Elsewhere, other S and SG products show similar or even greater dominance than the above products.

The third column of Fig. 6b illustrates the KGE produced by the best performer at each pixel and then compared with the KGE

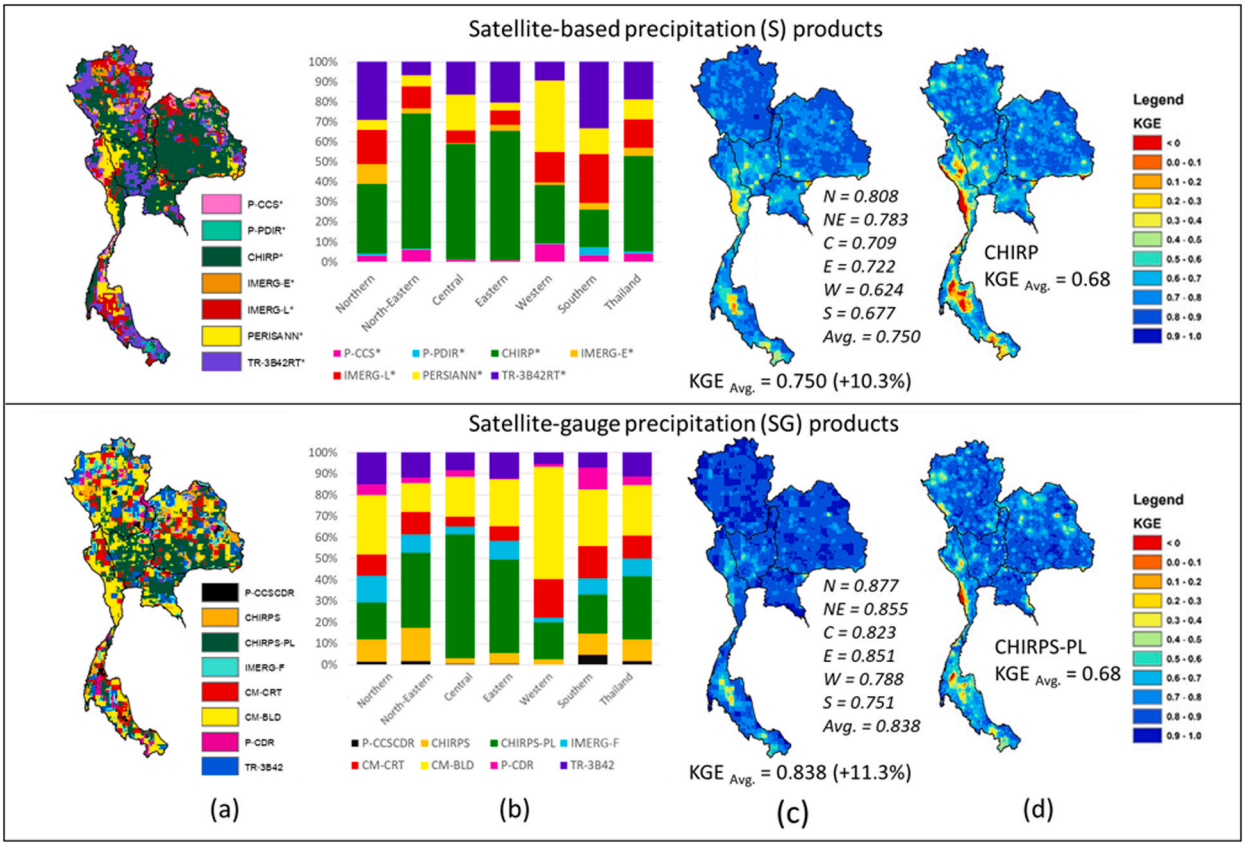

Fig. 6. **b** Performance of SPE Products in the S group (top) and SG group (bottom) across Thailand. (a) Spatial variation of SPE products producing the highest KGE at each pixel. (b) Cumulative bar plot showing the percentage of pixels identified as the best performer for each product across six regions of Thailand. (c) Highest KGE value for each pixel. (d) KGE values for each pixel for CHIRP and CHIRPS-Preliminary, which provide the highest average KGE values.

produced by the best-performing S and SG product, CHIRP and CHIRPS-Preliminary, respectively (as presented in the fourth column). The result of combining the best performer at each pixel enhanced the overall KGE for the S product group to 0.750, which is a 10.3 % improvement over CHIRP (KGE = 0.680). Similarly, an 11.3 % improvement was yielded for the SG product group – from 0.750 to 0.838.

Additional results in the form of heat maps of each statistical indicator at national and regional levels (Northern, Northeastern,

Table 3
Summary of the overall ranking of SPE products from performance evaluation.

SPE Products	Pixel to point				Pixel to pixel	Avg	Rank
	Four indicators	Taylor diagram	Effect of Elevation	Accuracy based on PDF	Four indicators		
CM-BLD	2	2	2	3	1	2.0	1
CHIRPS-PL	1	5	5	1	2	2.8	2
TR−3B42	3	3	1	4	4	3.0	3
IMERG-F	5	1	3	7	5	4.2	4
CM-CRT	4	4	9	2	3	4.4	5
CHIRPS	6	7	4	5	6	5.6	6
CHIRP*	7	8	8	6	7	7.2	7
P-CDR	8	6	6	11	9	8.0	8
TR−3B42RT*	9	9	7	8	11	8.8	9
IMERG-L*	11	11	11	12	8	10.6	10
IMERG-E*	12	10	10	13	10	11.0	11
PERSIANN*	10	12	13	9	12	11.2	12
P-CCS*	13	14	15	10	13	13.0	13
P-CCSCDR	14	13	12	14	14	13.4	14
P-PDIR*	15	15	14	15	15	14.8	15

Central, Eastern, Western and Southern Thailand) are presented in Figure S4 of the supplementary material. These scores show some variability across regions and products. In general, Northern Thailand provides better results, followed by Northeastern, Eastern, Central, Southern, and Western Thailand, respectively. Higher errors are observed near coastal areas, particularly in Southern and Western Thailand, which is consistent with the findings of Ventura (2020), who also evaluated different SPE products across Thailand. This is further supported by the research of Sun et al. (2018), which examined various SPE products globally and found that significant errors in rainfall estimates were particularly prominent over tropical oceans. This can be attributed to the fact that rainfall events over tropical oceans are primarily driven by convective systems, which exhibit high spatiotemporal variability (Pfeifroth et al., 2013).

To combine the performance of all indicators, each indicator was scaled (between 0 and 1) and averaged. These values are shown beneath the heat maps in Figure S4. CMORPH-BLD is the best performer at the nationwide level, providing the highest score of 0.946. This was followed by CHIRPS-Preliminary (0.925), CMORPH-CRT (0.883), and TRMM-3B42 (0.814). The four worst performing products are PERSIANN-PDIR (0.021), PERSIANN-CCSCDR (0.145), PERSIANN-CCS (0.346), and PERSIANN (0.472).

4.2.5. Overall ranking of SPE products

Based on the five criteria used to determine the accuracy of monthly SPE products within pixel-to-point and pixel-to-pixel comparisons, their overall performances were evaluated by scaling the score of each indicator. The SPE products were ranked, and the results are presented in Table 3. Here, CMORPH-BLD is the best performer. This is followed by CHIRPS-Preliminary, TRMM-3B42, GPM IMERG-Final, CMORPH-CRT, CHIRPS, and CHIRP, respectively. Meanwhile, the PERSIANN family products are the four worst performers, except for the PERSIANN-CDR which ranked eighth.

There are a few studies on SPE products in various catchments in Thailand, such as those conducted by Gunathilake et al. (2021), Gunathilake et al. (2020), Trang et al. (2020), and Li et al. (2019). These studies investigated different SPE products, primarily from the TRMM-3B42, GPM IMERG, and PERSIANN families. The TRMM-3B42 and GPM IMERG-Final products outperformed those from the PERSIANN family. These findings are consistent with the results presented in this study. Yang et al. (2021) is the only study to date that compares CMORPH-CRT and TRMM-3B42 for rainfall estimates across Thailand, finding that TRMM-3B42 was more accurate. Their results are consistent with our study, where TRMM-3B42 also outperformed CMORPH-CRT in rainfall estimates.

Several studies have evaluated the performance of different SPE products across countries outside of Thailand, and the results indicated that TRMM-3B42 generally performed well in several studies, including those by Awange and Forootan (2016); Li et al. (2015); Hu et al. (2014); Khan et al. (2014). After the release of GPM IMERG, its performance was found to be comparable to, or slightly better than, its predecessor, the TRMM-3B42 product (Le et al., 2020; Yang et al., 2020; Tang et al., 2020b; Yuan et al., 2017; Wang et al., 2017).

These results differ slightly from our study, as TRMM-3B42 performed marginally better than GPM IMERG. Among the studies conducted outside Thailand mentioned above, CMORPH-BLD was not included. In the studies comparing TRMM-3B42, GPM IMERG, CMORPH-BLD, and other products, CMORPH-BLD was generally superior in various areas (Xiang et al., 2021; Xiao et al., 2020), except for the study conducted in Northeastern China (Zhu et al., 2019), where TRMM-3B42 performed better. CHIRPS also performed well, ranking as the best product in the studies by Prakash (2019), Singh et al. (2024), and particularly in the global studies conducted by Sun et al. (2018), Beck et al. (2017) and Mazzoleni et al. (2019). These studies confirm the strong performance of CMORPH-BLD, which ranked first, and the CHIRP family, including CHIRPS-Preliminary, CHIRPS, and CHIRP, which ranked second, sixth, and seventh, respectively, among the fifteen products selected in this study. Overall, the performance of the PERSIANN family still lags behind other products (Singh et al., 2024; Ray et al., 2022; Mazzoleni et al.,2019; Beck et al., 2017), which is consistent with the results shown in this study.

It can be summarized that TRMM-3B42, GPM IMERG, CMORPH-BLD, and CHIRPS are among the top-performing products, as the data sources for these products are not drastically different—they primarily rely on infrared and microwave satellite data, although their algorithms differ. The choice of product mainly depends on the study area, as some products work better in specific regions while others may not perform as well.

4.3. Bias-correction of SPE products

4.3.1. Temporal cross-validation

The KGE between GGR and SPE data was improved after applying BC procedures. These improvements were quantified by comparing the bias-corrected SPE and GGR time series. The average results of repeating the process over the 180 sliding-windows of calibration and validation periods were also reported. A comparison of four BC procedures suggests that DTBC performs better than others across all SPE products, followed by QM, RABC and LBC, respectively. For the calibration period, the KGE of raw SPE products was 0.588 and was improved to 0.826, 0.804, 0.780, and 0.775, respectively. Similarly, for the validation period, KGE improved from 0.566 to 0.742, 0.740, 0.728, and 0.725, respectively. More information is available in Table S4 of the supplementary material.

The improved KGE results suggest the potential of all BC procedures in enhancing the accuracy of SPE products. After BC, CMORPH-BLD is the most reliable product, with a KGE of 0.891 and 0.807 during calibration and validation periods, respectively.

4.3.2. Spatial cross-validation

The KGE vlues of each left-out pixel, calculated based on the values of its eight surrounding pixels and averaged over the twenty repetitions ($KGE_{surrpix}$), were compared with the original KGE value ($KGE_{origpix}$) obtained in the temporal validation using the bias corrector(s) at that pixel. The average of $KGE_{surrpix}$ and $KGE_{origpix}$ across all pixels was calculated, which are denoted as $KGE_{surravg}$ and $KGE_{origavg}$, respectively.

Table S5 of supplementary material presents a comparison of $KGE_{surravg}$ and $KGE_{origavg}$ using the four BC procedures across all SPE products. It also includes percentage differences between $KGE_{surravg}$ and $KGE_{origavg}$ of the products. For SPE products, the $KGE_{surravg}$ and $KGE_{origavg}$ values as well as their differences appear to show some variability, albeit minor – with the reductions of KGE merely ranging between −2.7 % and −10.1 %. This indicates that, irrespective of the selected BC procedure, the bias correctors of surrounding pixels generally show adequate agreement.

However, unlike at the regional scale, it is inevitable that certain causative factors at more localised scales can lead to poor spatial cross-validation outcomes. As an example, the result of applying the DTBC procedure on CMORPH-BLD is presented in Figure S5. Panel a and b present the KGE distribution for the cases where the original data (100 % of stations) were included and where 30 % of stations were discarded (and gap-filled by the surrounding pixels), respectively. The average KGE dropped from 0.890 to 0.703. Panel C presents the KGE percentage changes, Panel D presents the topographic map of the area, and Panel E presents the annual rainfall over the study region. These plots suggest that the areas which coincide with heavy rainfall areas and complex topography – such as the west, upper northeast, east, and south regions, showed increasing error. These indicate the potential influence of orographic rainfall,

Table 4
Effects of the number of rainfall gauging stations on the accuracy of 15 bias-corrected SPE products.

	SPE Products	Raw	Percentage of gauge rainfall stations utilised in DTBC bias-correction procedure, (number of stations), and [the density of gauge rainfall station (km^2/station)]										
			5% (89) [5,779]	10% (178) [2,889]	20% (356) [1,445]	30% (543) [963]	40% (712) [722]	50% (890) [578]	60% (1,067) [482]	70% (1,245) [413]	80% (1,423) [361]	90% (1,601) [321]	**100 (1,779) [289]**
Satellite-based precipitation (S)	CHIRP*	0.678	0.695	0.716	0.735	0.746	0.753	0.761	0.766	0.769	0.773	0.776	**0.822**
			(2.5%)	(5.5%)	(8.4%)	(9.9%)	(11.0%)	(12.1%)	(12.9%)	(13.4%)	(13.9%)	(14.5%)	(21.2%)
	IMERG-L*	0.603	0.689	0.709	0.729	0.739	0.746	0.753	0.759	0.762	0.766	0.769	**0.822**
			(14.3%)	(17.7%)	(20.8%)	(22.6%)	(23.8%)	(25.0%)	(25.8%)	(26.4%)	(27.0%)	(27.5%)	(36.4%)
	IMERG-E*	0.582	0.684	0.704	0.723	0.733	0.740	0.748	0.753	0.756	0.759	0.763	**0.816**
			(17.5%)	(21.0%)	(24.2%)	(25.9%)	(27.1%)	(28.4%)	(29.2%)	(29.8%)	(30.4%)	(31.0%)	(40.0%)
	TR-3B42RT*	0.547	0.707	0.728	0.748	0.759	0.767	0.775	0.780	0.784	0.787	0.791	**0.843**
			(29.1%)	(33.0%)	(36.7%)	(38.7%)	(40.1%)	(41.5%)	(42.5%)	(43.1%)	(43.8%)	(44.5%)	(54.0%)
	PERSIANN*	0.540	0.633	0.651	0.668	0.676	0.683	0.689	0.693	0.696	0.699	0.702	**0.740**
			(17.2%)	(20.6%)	(23.6%)	(25.2%)	(26.3%)	(27.4%)	(28.3%)	(28.8%)	(29.4%)	(29.9%)	(36.9%)
	P-CCS*	0.468	0.635	0.654	0.672	0.681	0.687	0.693	0.698	0.702	0.705	0.708	**0.747**
			(35.7%)	(39.7%)	(43.4%)	(45.3%)	(46.6%)	(48.0%)	(49.1%)	(49.8%)	(50.5%)	(51.1%)	(59.4%)
	P-PDIR*	0.357	0.623	0.641	0.658	0.666	0.672	0.678	0.683	0.685	0.688	0.691	**0.726**
			(74.4%)	(79.5%)	(84.1%)	(86.5%)	(88.2%)	(89.8%)	(91.1%)	(91.8%)	(92.7%)	(93.4%)	(103.2%)
Satellite-gauge precipitation (SG)	CHIRPS-PL	0.753	0.722	0.744	0.765	0.776	0.784	0.793	0.799	0.802	0.806	0.810	**0.870**
			(-4.1%)	(-1.2%)	(1.6%)	(3.1%)	(4.2%)	(5.3%)	(6.0%)	(6.5%)	(7.1%)	(7.6%)	(15.6%)
	CM-BLD	0.744	0.737	0.760	0.782	0.794	0.802	0.811	0.817	0.821	0.825	0.829	**0.896**
			(-1.0%)	(2.1%)	(5.0%)	(6.6%)	(7.7%)	(8.9%)	(9.7%)	(10.3%)	(10.8%)	(11.4%)	(20.3%)
	CM-CRT	0.708	0.726	0.748	0.769	0.780	0.789	0.797	0.803	0.806	0.811	0.814	**0.870**
			(2.6%)	(5.7%)	(8.7%)	(10.3%)	(11.4%)	(12.6%)	(13.4%)	(14.0%)	(14.5%)	(15.1%)	(22.9%)
	TR-3B42	0.700	0.735	0.757	0.779	0.791	0.799	0.808	0.814	0.818	0.822	0.826	**0.890**
			(5.0%)	(8.2%)	(11.4%)	(13.0%)	(14.2%)	(15.5%)	(16.3%)	(16.9%)	(17.5%)	(18.1%)	(27.2%)
	IMERG-F	0.664	0.732	0.755	0.777	0.788	0.797	0.805	0.811	0.815	0.819	0.823	**0.887**
			(10.3%)	(13.7%)	(16.9%)	(18.7%)	(20.0%)	(21.2%)	(22.1%)	(22.7%)	(23.4%)	(24.0%)	(33.6%)
	CHIRPS	0.663	0.722	0.743	0.764	0.776	0.784	0.792	0.798	0.801	0.806	0.810	**0.872**
			(8.9%)	(12.0%)	(15.2%)	(16.9%)	(18.1%)	(19.4%)	(20.2%)	(20.8%)	(21.4%)	(22.0%)	(31.5%)
	P-CDR	0.536	0.708	0.730	0.750	0.761	0.768	0.776	0.782	0.785	0.789	0.793	**0.841**
			(32.1%)	(36.1%)	(39.9%)	(41.9%)	(43.3%)	(44.7%)	(45.8%)	(46.4%)	(47.1%)	(47.8%)	(56.8%)
	P-CCSCDR	0.349	0.682	0.702	0.721	0.731	0.738	0.745	0.750	0.753	0.756	0.760	**0.809**
			(95.0%)	(100.8%)	(106.2%)	(109.1%)	(111.0%)	(113.0%)	(114.5%)	(115.4%)	(116.4%)	(117.4%)	(131.4%)
S	**Avg.**	**0.54**	**0.667**	**0.686**	**0.705**	**0.714**	**0.721**	**0.728**	**0.733**	**0.736**	**0.74**	**0.743**	**0.788**
			(23.6%)	(27.2%) 3.0%	(30.6%) 2.6%	(32.4%) 1.4%	(33.6%) 0.9%	(34.9%) 1.0%	(35.8%) 0.7%	(36.4%) 0.4%	(37.1%) 0.5%	(37.7%) 0.4%	(46.0%)
SG	**Avg.**	**0.64**	**0.721**	**0.742**	**0.763**	**0.775**	**0.783**	**0.791**	**0.797**	**0.8**	**0.804**	**0.808**	**0.867**
			(12.6%)	(16.0%) 3.0%	(19.3%) 2.8%	(21.1%) 1.5%	(22.3%) 1.0%	(23.6%) 1.0%	(24.5%) 0.7%	(25.1%) 0.5%	(25.7%) 0.5%	(26.3%) 0.5%	(35.5%)

Note: The number in the bracket indicates the percentage of improvement of KGE compared with the KGE of raw data. The percentage number in no bracket with underline indicates the percentage of improvement of KGE compared with previous cases.

which creates steeper localised rainfall gradients around watershed boundaries. In southern Thailand, oceanic influences are likely to be an additional contributor to the reduced KGE. This, in turn, affects the validity of the bias correctors of the surrounding pixels used for gap-filling the left-out pixels in these areas.

4.4. *Effects of the number of gauged rainfall stations on the accuracy of bias-corrected SPE products*

The effects of the density of gauged rainfall stations on the KGE resulting from applying the DTBC method is shown in Table 4. The GGR_{100} dataset established in Step 1 yielded KGE of 0.788 for S products and 0.867 for SG products. In Step 2, several noteworthy observations were made with regards to KGE improvements:

- Considerable improvements to raw accuracy were yielded by BC using GGR_5 (89 out of 1779 stations / 5779 km^2/station), with S and SG products yielding an average gain of 23.6 % and 12.6 %, respectively. Notably, this improved the average KGE of S products to 0.667, which exceeds the accuracy of raw SG products (0.64).
- Similarly, the improvement of average KGE of SG products to 0.721 using GGR_5 provides equivalent outcomes to performing BC on S products using GGR_{40} (712 out of 1779 stations / 722 km^2/station).

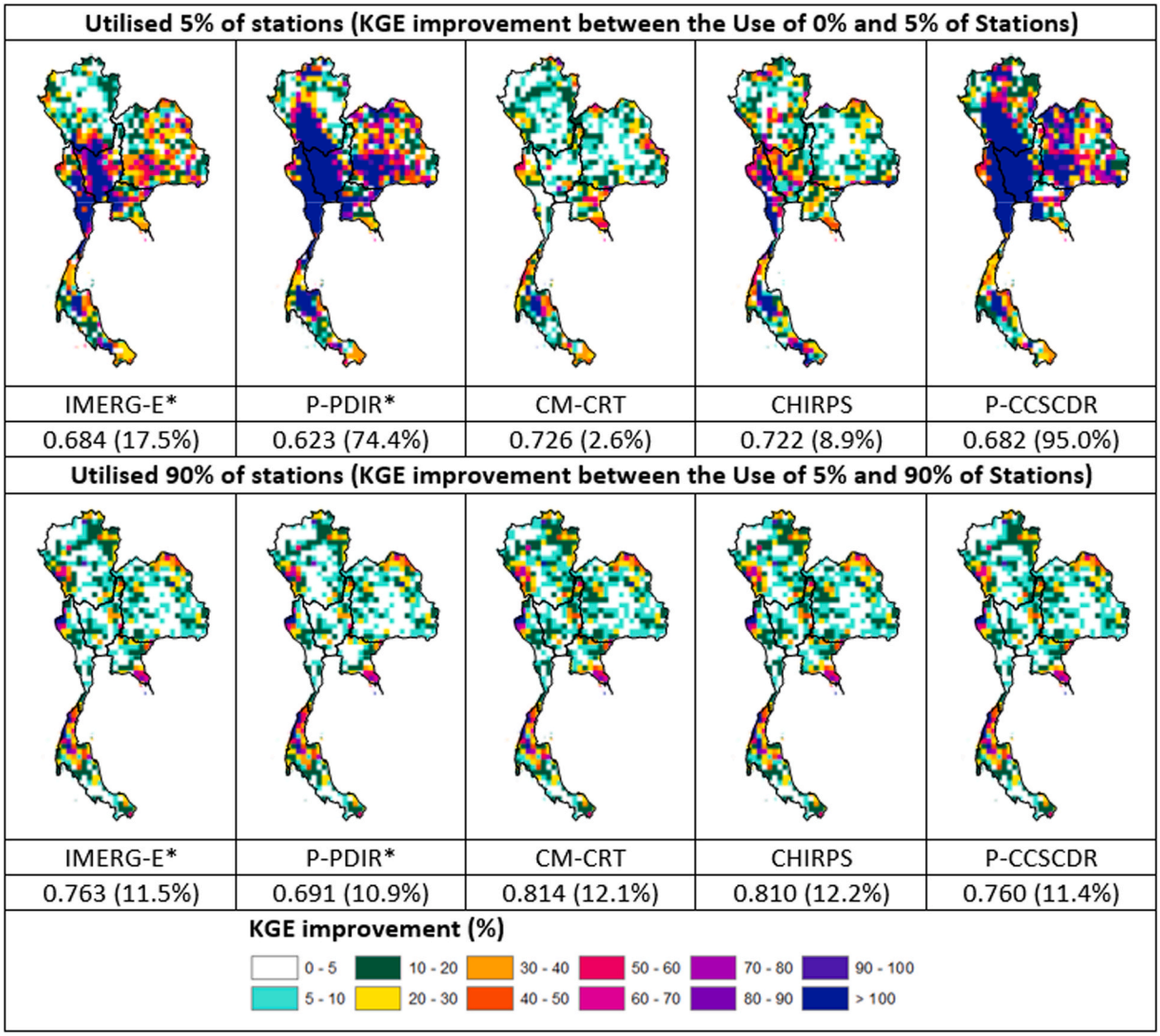

Fig. 7. Spatial variability of the KGE improvements for the cases where the DTBC procedure was performed on selected SPE products using GGR_5 and GGR_{90}.

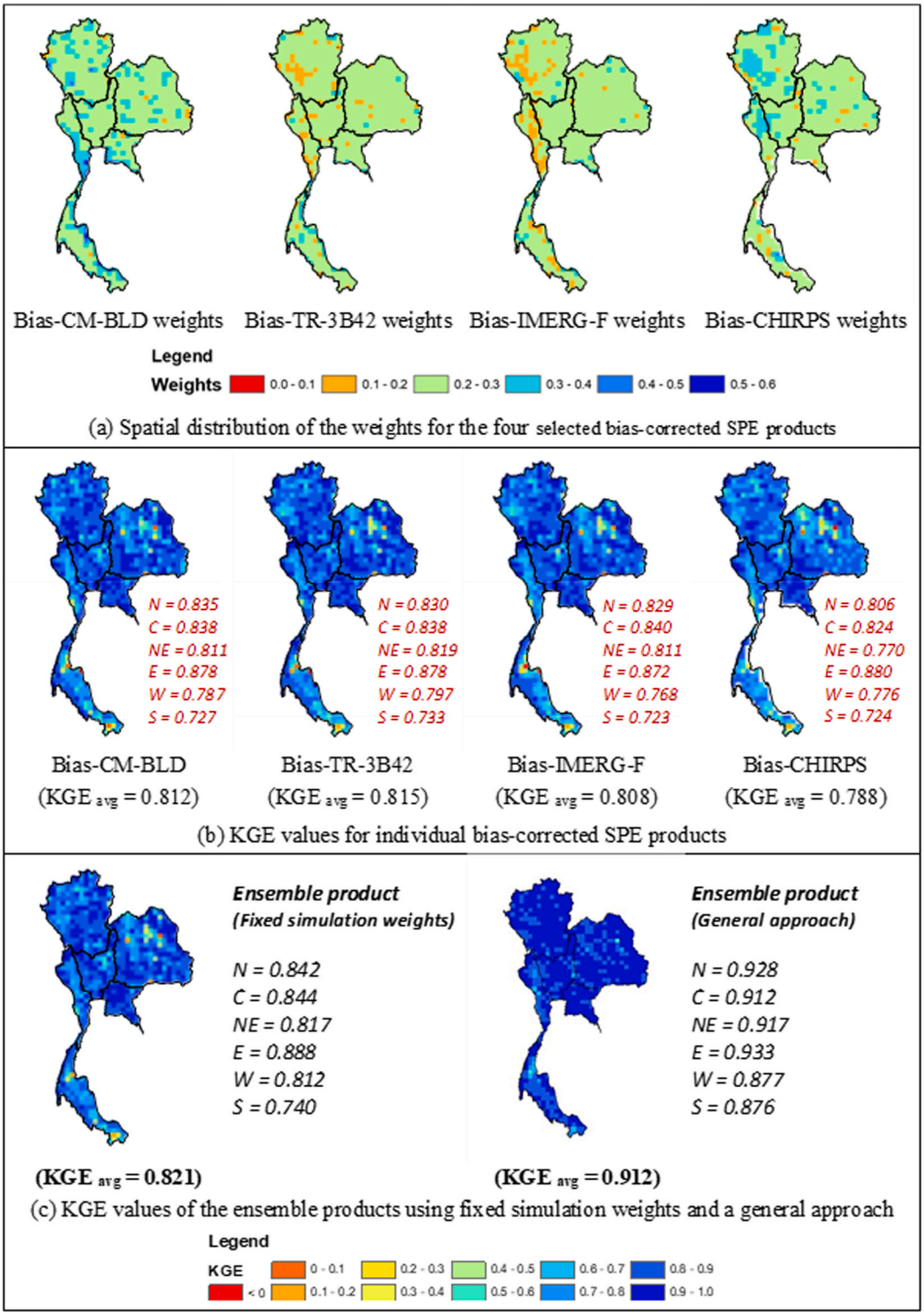

Fig. 8. Generation of an ensemble bias-corrected SPE product. (a) Spatial distribution of the weights for the four selected bias-corrected SPE products. (b) KGE values for individual bias-corrected SPE products. (c) KGE values of the ensemble products using fixed simulation weights and a general approach.

- As the percentage of stations in the GGR dataset is incrementally increased, the KGE improvements gradually reach to an optimal stage. For instance, the improvement achieved by BC using GGR_{90} were 37.7 % and 26.3 % for S and SG products, respectively, which are merely approx. 14 % further increases relative to using GGR_5.

Fig. 7 presents the spatial variability of the KGE improvements for selected products for the cases where DTBC was performed using GGR_5 and GGR_{90}.

- The first row presents the KGE improvements provided by GGR_5. PERSIANN-PDIR and PERSIANN-CCSCDR yielded improvements of 74.4 % and 95.0 %, respectively, while CMORPH-CRT, CHIRPS, and GPM IMERG-Early improved by 2.6 %, 8.9 % and 17.5 %, respectively. This indicates that this can greatly improve accuracies in areas where SPE products may exhibit significant underlying biases.
- The second row shows that by applying GGR_{90}, each product yielded consistent additional improvements of approx. 11–12 % relative to the accuracy achieved by applying GGR_5. Here, the notable similarities in spatial variation of improvements indicates that the BC of raw SPE products using GGR_5 (89 out of 1779 stations) suffices at preliminarily assimilating bias-prone SPE estimates towards gauged rainfall estimate, such that the corrected SPE estimates show little discrepancy across different products.

Arguably, this demonstrates that the merit of extensively including gauged rainfall data in BC procedures is of lesser significance than the attainable benefits of undertaking this fundamental exercise despite potential constraints in data availability.

4.5. Generation of an ensemble bias-corrected SPE product

Fig. 8 presents a comparison of KGE values of four selected products on an individual basis and, also for the case when KGE is estimated from the weighted averaged time series. The first row shows the spatial distribution of the weights for the four products. It can be observed that many pixels have nearly equal weights, with Bias-CHIRPS and Bias-CMORPH-BLD receiving higher weights in many pixels in the Northern region. Bias-CMORPH-BLD also received more weight in the Central region. The second row compares the KGE values of the individual products. Overall, these bias-corrected SPE (BSPE) products perform similarly, except in a few locations where their performance is moderate. The left panel of the last row shows the spatial distribution of KGE derived from the weighted time series. As expected, the weighted time series provides better results compared to the individual products for the overall pixels. Regionally, all BSPE products show an improvement of 3.9 % in the Western region, 1.1 % in the Central region, and 1.9 % across the overall area. Although the accuracy improvement in KGE values is modest compared to using individual products, fixed simulation weights for each product and pixel can be applied to future rainfall data for the four selected products used to create the ensemble.

In general, an ensemble product is used to achieve the highest accuracy for historical rainfall data. In this case, the weights assigned to each pixel and product can vary from month to month throughout the overall period, as typically done in previous studies (Muhammad et al., 2018; Rahman et al., 2018; Beck et al., 2017; Poortinga et al., 2017). Following this general approach, the most accurate ensemble product is also shown in Fig. 8. The results demonstrate that the average KGE value for the entire area increases to 0.912, compared to 0.821 when using fixed simulation weights for each product and pixel. However, the primary objective of this study is to identify fixed simulation weights for creating future ensemble products, which is not typically addressed in previous studies.

4.6. Limitations and Further Study

In this study, we conducted a comprehensive evaluation of the accuracy of satellite-based precipitation estimates over Thailand using monthly data. While the results presented here may be similar to those obtained with daily data, there may be differences in specific details. Further research using these fifteen SPE products could provide a more in-depth analysis of rainfall intensity, the number of rainfall days, rainfall detection probability, and extreme rainfall events, which have a significant impact on flood management. An alternative approach to evaluate the accuracy of daily SPE products could involve using a hydrological model, as the biases present in daily SPE products can be difficult to eliminate in daily data but may be more easily addressed through a hydrological model. This would enhance the usefulness of daily SPE products in providing runoff estimates, especially in areas with limited daily rainfall data.

5. Discussions

An appropriate selection of SPE products is a multi-faceted decision-making exercise that requires critical evaluation of several factors that can influence performance. Particularly for regions where gauged rainfall data availability is scarce, it is worthy to understand the crucial factors that can help ensure our ability to implement SPE products with adequate confidence. A thorough assessment of the performance of SPE product was undertaken and important aspects were noted.

Overall, CHIRPS-Preliminary appeared to be a praiseworthy product despite not being selected to form the ensemble product as it performed ever-so-slightly poorer than its counterpart CHIRPS after applying DTBC (KGE = 0.781 vs 0.783). During the pixel-to-pixel comparison, CHIRPS-Preliminary was ranked as the best performer across 29.6 % of pixels in the study area (CMORPH-BLD and TRMM-3B42 follow with 23.7 % and 11.2 %, respectively). Its fine spatial resolution of 5 km and short latency period of two days provides added operational benefits in comparison to the final ensemble product (25 km), which only has a marginal edge in accuracy (KGE = 0.821) and its lengthy latency period of three months and greater.

SPE products of the PERSIANN family, which yielded the lowest accuracies in the performance evaluation exercise, in turn appeared to benefit significantly from BC (e.g., PERSIANN-PDIR showed KGE = 0.639). Given its latency period of 15–60 minutes relative to the best-performing S product (TRMM-3B42RT = 0.759) and most notably its efficacy for capturing rainfall extremes, PERSIANN-PDIR offers a great promise for use in near-real-time flood warning.

The study also demonstrated that the quality of gauged rainfall data used to form the GGR dataset has the capability to undermine accuracy outcomes achieved from performing bias correction. The widespread availability of gauged rainfall data in the study area provided the opportunity to develop an understanding on implementing the SPE products in case of dataset limitations. Promisingly, Section 4.4 suggests that sufficient improvements to accuracies of raw SPE products are achievable despite limitations in data availability.

It was shown that the bias correction using 5 % of raingauges (GGR_5) has the capability of enhancing accuracies of raw S products – indicating that improvements are possible even if observations are limited. The availability of a well distributed observational network ensures that the spatiotemporal variation of rainfall, specifically caused by factors at local scales such as orographic effects, is adequately captured. Pixel-to-pixel and pixel-to-point evaluation of SPE products were conducted. On an overall basis, not much difference in performance was noted (varies from 72 % (pixel-to-point) to 75 % (pixel-to-pixel). There could be differences on a regional scale and/or extreme events which were not examined in this research.

An ensemble product has been developed using top-performing bias-corrected SPE products, yielding KGE values ranging from 0.788 to 0.815. By applying fixed simulation weights, the KGE improved by 1 %–4 %, reaching 0.821. Additionally, an ensemble with varying weights was explored, achieving an even higher KGE of 0.906 for historical rainfall data. While these results demonstrate notable improvements, the primary objective of this study is to identify fixed simulation weights for future ensemble products. This focus on fixed weights for future applications distinguishes the study from prior research, which has not thoroughly addressed this aspect.

6. Conclusions

The study presents a framework for evaluating and ranking the performance of fifteen SPE products across river basins in Thailand, using both pixel-to-point and pixel-to-pixel comparisons based on multiple criteria. The preparation of quality-assured gauged rainfall data from 1779 stations, through 14 comprehensive quality control steps, provided a reliable foundation for the performance evaluations and facilitated the appropriate selection of SPE products. The study's first finding reveals that CMORPH-BLD is the top performer, followed by CHIRPS-Preliminary, TRMM-3B42, GPM IMERG-Final, CMORPH-CRT, CHIRPS, and CHIRP.

The second objective of this study focused on evaluating the accuracy of the SPE products in relation to rainfall frequency and elevation. The results showed that rainfall estimates from the SPE products were generally underestimated at rare probabilities and overestimated at more frequent probabilities. In contrast, PERSIANN-PDIR and PERSIANN-CCSCDR showed relatively lower errors for these rare events, indicating superior performance in detecting extreme monthly rainfall. These findings align with those of previous studies (Baig et al., 2023; Sadeghi et al., 2021; Jiang et al., 2019; Huang et al., 2018; Tan et al., 2015).

The impact of elevation on the performance of SPE products results in relatively lower accuracies near sea level (0–200 m, with an average KGE of 0.62 for the top five performers), with accuracy stabilizing between 200 and 800 m (KGE = 0.71). The higher density of gauged rainfall stations at lower elevations enhances the reliability of the data. Accuracy decreases for the elevation bands 800–1000 m and > 1000 m (KGE = 0.68 and 0.54, respectively), where the number of gauged rainfall stations is minimal (0.8 % and 0.4 %, respectively), leading to increased uncertainties in assessing SPE product performance at higher elevations. These findings are consistent with those of Amjad et al. (2020), who reported a slight decline in monthly rainfall accuracy for SPE products in areas with slopes greater than 15 %, compared to the overall gauged rainfall stations.

The third objective of this study was to examine how the number of gauged rainfall stations influences the accuracy of bias-corrected SPE products. The overall results demonstrated that bias correction improves the performance of all SPE products. Additionally, when only 5 % of the available rainfall stations (out of 1779) from each of the 22 sub-basins in Thailand are used (approximately 5800 km^2 per station), the accuracy of most SPE products improves significantly compared to their non-bias-corrected versions, particularly for the S products. These findings suggest that bias correction alone is sufficient to enhance accuracy, especially in regions with sparse rainfall gauge networks.

The final objective of the study was to develop an ensemble product using the top-performing bias-corrected SPE products, as individual products performed differently across locations. The four top-performing bias-corrected SPE products—Bias-TRMM-3B42, Bias-CMORPH-BLD, Bias-GPM IMERG-Final, and Bias-CHIRPS—had KGE values ranging from 0.788 to 0.815 on average across Thailand. In contrast, the ensemble product, derived using fixed simulation weights, achieved a higher average KGE of 0.821, representing a 1 %–4 % improvement. Although overall accuracy did not show a significant improvement across all areas, regional improvements were notable, particularly in the Western region. The results suggest that the weighted ensemble outperforms individual products at all pixels. Furthermore, fixed simulation weights can be reliably applied to future rainfall data for the four selected products used to create the ensemble. The findings confirm the robustness of fixed simulation weights for future application, an aspect that has not typically been evaluated in previous studies.

CRediT authorship contribution statement

Nutchanart Sriwongsitanon: Writing – review & editing, Writing – original draft, Visualization, Supervision, Resources, Project administration, Methodology, Funding acquisition, Formal analysis, Conceptualization. **Chainarong Ophaphaibun:** Visualization,

Software, Formal analysis, Data curation. **Rajeshwar Mehrotra:** Writing – review & editing, Visualization, Methodology, Conceptualization. **James Alexander Williams:** Writing – review & editing, Writing – original draft, Visualization, Validation, Software, Resources, Methodology, Formal analysis. **Chanphit Kaprom:** Writing – original draft, Visualization, Validation, Supervision, Software, Resources, Methodology, Investigation, Formal analysis, Data curation, Conceptualization.

Declaration of Competing Interest

The authors declare that they have no known competing financial interests or personal relationships that could have appeared to influence the work reported in this paper

Acknowledgements

The authors gratefully acknowledge Remote Sensing Research Centre for Water Resources Management SENSWAT, Faculty of Engineering, Kasetsart University for financially supporting this research. We also appreciate Royal Irrigation Department and Thai Meteorology Department for providing the daily rainfall data. We truthfully thank the Climate Hazards Group, National Aeronautics and Space Administration (NASA), Japan Aerospace Exploration Agency (JAXA), Center for Hydrometeorology and Remote Sensing (CHRS) and National Oceanic and Atmospheric Administration (NOAA) for creating and sharing the RS rainfall data to be used in this study. We gratefully received funding from the Master's Degree Education Promotion Program, Plan A, Faculty of Engineering, Kasetsart University. Finally, the authors gratefully acknowledge the constructive comments and suggestions provided by the reviewers, which have significantly contributed to the enhancement of this manuscript.

Appendix A. Supporting information

Supplementary data associated with this article can be found in the online version at doi:10.1016/j.ejrh.2025.102380.

Data availability

Data will be made available on request.

References

Abbott, P.F., 1986. Guidelines on the quality control of surface climatological data. WMO/TD-No.111, World Meteorological Organization, Geneva, Switzerland.
AghaKouchak, A., Behrangi, A., Sorooshian, S., Hsu, K., Amitai, E., 2011. Evaluation of satellite-retrieved extreme precipitation rates across the central United States. J. Geophys. Res.: Atmos. 116 (D2). https://doi.org/10.1029/2010JD014741.
Al-Dousari, A., Ramdan, A., Al Ghadban, A., 2008. Site-specific precipitation estimate from TRMM data using bilinear weighted interpolation technique: An example from Kuwait. J. Arid Environ. 72 (7), 1320–1328. https://doi.org/10.1016/j.jaridenv.2007.12.013.
Amjad, M., Yilmaz, M.T., Yucel, I., Yilmaz, K.K., 2020. Performance evaluation of satellite-and model-based precipitation products over varying climate and complex topography. J. Hydrol. 584, 124707. https://doi.org/10.1016/j.jhydrol.2020.124707.
Anjum, M.N., Ding, Y., Shangguan, D., Ijaz, M.W., Zhang, S., 2016. Evaluation of high-resolution satellite-based real-time and post-real-time precipitation estimates during 2010 extreme flood event in Swat River Basin, Hindukush region. Adv. Meteor. 2016. https://doi.org/10.1155/2016/2604980.
Aryal, A., Tran, T.N.D., Kumar, B., Lakshmi, V., 2023. Evaluation of satellite-derived precipitation products for streamflow simulation of a mountainous himalayan watershed: a study of Myagdi Khola in Kali Gandaki Basin, Nepal. Remote Sens 15 (19), 4762. https://doi.org/10.3390/rs15194762.
Awange, J.L., Forootan, E., 2016. An evaluation of high-resolution gridded precipitation products over Bhutan (1998-2012). Int. J. Clim. 36 (3). https://doi.org/10.1002/joc.4402.
Bai, X., Wu, X., Wang, P., 2019. Blending long-term satellite-based precipitation data with gauge observations for drought monitoring: Considering effects of different gauge densities. J. Hydrol. 577, 124007. https://doi.org/10.1016/j.jhydrol.2019.124007.
Baig, F., Abrar, M., Chen, H., Sherif, M., 2023. Evaluation of precipitation estimates from remote sensing and artificial neural network based products (PERSIANN) family in an arid region. Remote Sens 15 (4), 1078. https://doi.org/10.3390/rs15041078.
Beck, H.E., Van Dijk, A.I., Levizzani, V., Schellekens, J., Miralles, D.G., Martens, B., De Roo, A., 2017. MSWEP: 3-hourly 0.25 global gridded precipitation (1979–2015) by merging gauge, satellite, and reanalysis data. Hydrol. Earth Syst. Sci. 21 (1), 589–615. https://doi.org/10.5194/hess-21-589-2017.
Behrangi, A., Wen, Y., 2017. On the spatial and temporal sampling errors of remotely sensed precipitation products. Remote Sens 9 (11), 1127. https://doi.org/10.3390/rs9111127.
Bhatti, H.A., Rientjes, T., Haile, A.T., Habib, E., Verhoef, W., 2016. Evaluation of bias correction method for satellite-based rainfall data. Sens 16 (6), 884. https://doi.org/10.3390/s16060884.
Bouwer, L.M., Aerts, J.C.J.H., Coterlet, G.V.D., Giesen, N.V.D., Gieske, A., Mannaerts, C., 2004. Evaluating downscaling methods for preparing global circulation model (GCM) data for hydrological impact modelling, in:Climate change in contrasting river basins: adaptation strategies for water, food and environment. CABI Publishing, Wallingford UK, pp. 25–47. https://doi.org/10.1079/9780851998350.0025.
Cannon, A.J., Sobie, S.R., Murdock, T.Q., 2015. Bias correction of GCM precipitation by quantile mapping: how well do methods preserve changes in quantiles and extremes? J. Clim. 28 (17), 6938–6959. https://doi.org/10.1175/JCLI-D-14-00754.1.
Chaudhary, S., Dhanya, C.T., 2019. Investigating the performance of bias correction algorithms on satellite-based precipitation estimates. Remote Sens. Agric. Ecosys. Hydrol. Xxi. Proc. SPIE 11149, 279–285. https://doi.org/10.1117/12.2533214.
Cheema, M.J.M., Bastiaanssen, W.G.M., 2012. Local calibration of remotely sensed rainfall from the TRMM satellite for different periods and spatial scales in the Indus Basin. Int. J. Remote Sens 33 (8), 2603–2627. https://doi.org/10.1080/01431161.2011.617397.
Chen, J., Brissette, F.P., Chaumont, D., Braun, M., 2013. Finding appropriate bias correction methods in downscaling precipitation for hydrologic impact studies over North America. Water Resour. Res. 49 (7), 4187–4205. https://doi.org/10.1002/wrcr.20331.
Deng, S., Chen, T., Yang, N., Qu, L., Li, M., Chen, D., 2018. Spatial and temporal distribution of rainfall and drought characteristics across the Pearl River basin. Sci. Total Environ. 619, 28–41. https://doi.org/10.1016/j.scitotenv.2017.10.339.

Derin, Y., Anagnostou, E., Berne, A., Borga, M., Boudevillain, B., Buytaert, W., Chang, C.H., Chen, H., Delrieu, G., Hsu, Y.C., Lavado-Casimiro, W., 2019. Evaluation of GPM-era global satellite precipitation products over multiple complex terrain regions. Remote Sens 11 (24), 2936. https://doi.org/10.3390/rs11242936.
Duan, Z., Bastiaanssen, W.G.M., 2013. First results from Version 7 TRMM 3B43 precipitation product in combination with a new downscaling–calibration procedure. Remote Sens. Environ. 131, 1–13. https://doi.org/10.1016/j.rse.2012.12.002.
Duan, Z., Liu, J., Tuo, Y., Chiogna, G., Disse, M., 2016. Evaluation of eight high spatial resolution gridded precipitation products in Adige Basin (Italy) at multiple temporal and spatial scales. Sci. Total Environ. 573, 1536–1553. https://doi.org/10.1016/j.scitotenv.2016.08.213.
Ebert, E.E., Janowiak, J.E., Kidd, C., 2007. Comparison of near-real-time precipitation estimates from satellite observations and numerical models. Bull. Am. Meteorol. Soc. 88 (1), 47–64. https://doi.org/10.1175/BAMS-88-1-47.
Eini, M.R., Rahmati, A., Piniewski, M., 2022. Hydrological application and accuracy evaluation of PERSIANN satellite-based precipitation estimates over a humid continental climate catchment. J. Hydrol.: Reg. Stud. 41, 101109. https://doi.org/10.1016/j.ejrh.2022.101109.
Enayati, M., Bozorg-Haddad, O., Bazrafshan, J., Hejabi, S., Chu, X., 2021. Bias correction capabilities of quantile mapping methods for rainfall and temperature variables. J. Water Clim. Chang 12 (2), 401–419. https://doi.org/10.2166/wcc.2020.261.
Funk, C., Michaelsen, J., Marshall, M.T., 2012. Mapping recent decadal climate variations in precipitation and temperature across eastern Africa and the Sahel. Remote Sens. Drought.: Innov. Monit. Approaches 331. ⟨https://digitalcommons.unl.edu/usgsstaffpub/977⟩.
Funk, C., Peterson, P., Landsfeld, M., Pedreros, D., Verdin, J., Shukla, S., Husak, G., Rowland, J., Harrison, L., Hoell, A., Michaelsen, J., 2015. The climate hazards infrared precipitation with stations—a new environmental record for monitoring extremes. Sci. Data 2 (1), 1–21. https://doi.org/10.1038/sdata.2015.66.
Gottardi, F., Obled, C., Gailhard, J., Paquet, E., 2012. Statistical reanalysis of precipitation fields based on ground network data and weather patterns: Application over French mountains. J. Hydrol. 432, 154–167. https://doi.org/10.1016/j.jhydrol.2012.02.014.
Gudmundsson, L., Bremnes, J.B., Haugen, J.E., Engen-Skaugen, T., 2012. Downscaling RCM precipitation to the station scale using statistical transformations–a comparison of methods. Hydrol. Earth Syst. Sci. 16 (9), 3383–3390. https://doi.org/10.5194/hess-16-3383-2012.
Gumindoga, W., Rientjes, T.H.M., Haile, A.T., Makurira, H., Reggiani, P., 2019. Performance of bias-correction schemes for CMORPH rainfall estimates in the Zambezi River basin. Hydrol. Earth Syst. Sci. 23 (7), 2915–2938. https://doi.org/10.5194/hess-23-2915-2019.
Gunathilake, M.B., Amaratunga, Y.V., Perera, A., Karunanayake, C., Gunathilake, A.S., Rathnayake, U., 2020. Statistical evaluation and hydrologic simulation capacity of different satellite-based precipitation products (SbPPs) in the Upper Nan River Basin, Northern Thailand. J. Hydrol.: Reg. Stud. 32, 100743. https://doi.org/10.1016/j.ejrh.2020.100743.
Gunathilake, M.B., Zamri, M.N.M., Alagiyawanna, T.P., Samarasinghe, J.T., Baddewela, P.K., Babel, M.S., Jha, M.K., Rathnayake, U.S., 2021. Hydrologic utility of satellite-based and gauge-based gridded precipitation products in the Huai Bang Sai Watershed of Northeastern Thailand. Hydrol 8 (4), 165. https://doi.org/10.3390/hydrology8040165.
Guo, H., Bao, A., Ndayisaba, F., Liu, T., Kurban, A., De Maeyer, P., 2017. Systematical evaluation of satellite precipitation estimates over central Asia using an improved error-component procedure. J. Geophys. Res.: Atmos. 122 (20), 10–906. https://doi.org/10.1002/2017JD026877.
Gupta, H.V., Kling, H., Yilmaz, K.K., Martinez, G.F., 2009. Decomposition of the mean squared error and NSE performance criteria: Implications for improving hydrological modelling. J. Hydrol. 377 (1-2), 80–91. https://doi.org/10.1016/j.jhydrol.2009.08.003.
Habib, E., Haile, A.T., Sazib, N., Zhang, Y., Rientjes, T., 2014. Effect of bias correction of satellite-rainfall estimates on runoff simulations at the source of the Upper Blue Nile. Remote Sens 6 (7), 6688–6708. https://doi.org/10.3390/rs6076688.
Hamada, A., Arakawa, O., Yatagai, A., 2011. An automated quality control method for daily rain-gauge data. Glob. Environ. Res. 15 (2), 183–192.
Hsu, K.L., Gao, X., Sorooshian, S., Gupta, H.V., 1997. Precipitation estimation from remotely sensed information using artificial neural networks. J. Appl. Meteor. 36 (9), 1176–1190. https://doi.org/10.1175/1520-0450(1997)036< 1176:PEFRSI> 2.0.CO;2.
Hu, Q., Yang, D., Li, Z., Mishra, A.K., Wang, Y., Yang, H., 2014. Multi-scale evaluation of six high-resolution satellite monthly rainfall estimates over a humid region in China with dense rain gauges. Int. J. Remote Sens 35 (4), 1272–1294. https://doi.org/10.1080/01431161.2013.876118.
Huang, X., Wang, D., Liu, Y., Feng, Z., Wang, D., 2018. Evaluation of extreme precipitation based on satellite retrievals over China. Front. Earth Sci. 12, 846–861. https://doi.org/10.1007/s11707-017-0643-2.
Huffman, G.J., Bolvin, D.T., 2013. GPCP version 2.2 SG combined precipitation data set documentation. NASA GSFC Doc. 46.
Huffman, G.J., Bolvin, D.T., Nelkin, E.J., Wolff, D.B., Adler, R.F., Gu, G., Hong, Y., Bowman, K.P., Stocker, E.F., 2007. The TRMM Multisatellite Precipitation Analysis (TMPA): Quasi-global, multiyear, combined-sensor precipitation estimates at fine scales. J. Hydrometeorol. 8 (1), 38–55. https://doi.org/10.1175/JHM560.1.
Huffman, G.J., Adler, R.F., Bolvin, D.T., Nelkin, E.J., 2010. The TRMM Multi-Satellite Precipitation Analysis (TMPA). In: Gebremichael, M., Hossain, F. (Eds.), Satellite Rainfall Applications for Surface Hydrology. Springer, Dordrecht. https://doi.org/10.1007/978-90-481-2915-7_1.
Huffman, G.J., Bolvin, D.T., Nelkin, E.J., Tan, J., 2015. Integrated Multi-satellitE Retrievals for GPM (IMERG) technical documentation. NASA/GSFC Code 612 (47), 2019.
Javanmard, S., Yatagai, A., Nodzu, M.I., BodaghJamali, J., Kawamoto, H., 2010. Comparing high-resolution gridded precipitation data with satellite rainfall estimates of TRMM_3B42 over Iran. Adv. Geosci. 25, 119–125. https://doi.org/10.5194/adgeo-25-119-2010.
Jiang, Q., Li, W., Wen, J., Fan, Z., Chen, Y., Scaioni, M., Wang, J., 2019. Evaluation of satellite-based products for extreme rainfall estimations in the eastern coastal areas of China. J. Integr. Environ. Sci. 16 (1), 191–207. https://doi.org/10.1080/1943815X.2019.1707233.
Jiang, S., Ren, L., Xu, C.Y., Yong, B., Yuan, F., Liu, Y., Yang, X., Zeng, X., 2018. Statistical and hydrological evaluation of the latest Integrated Multi-satellitE Retrievals for GPM (IMERG) over a midlatitude humid basin in South China. Atmos. Res. 214, 418–429. https://doi.org/10.1016/j.atmosres.2018.08.021.
Jiang, S.H., Zhou, M., Ren, L.L., Cheng, X.R., Zhang, P.J., 2016. Evaluation of latest TMPA and CMORPH satellite precipitation products over Yellow River Basin. Water Sci. Eng. 9 (2), 87–96. https://doi.org/10.1016/j.wse.2016.06.002.
Jiang, Y., Yang, K., Qi, Y., Zhou, X., He, J., Lu, H., Li, X., Chen, Y., Li, X., Zhou, B., Mamtimin, A., 2023. TPHiPr: a long-term (1979–2020) high-accuracy precipitation dataset (1/30◦, daily) for the Third Pole region based on high-resolution atmospheric modeling and dense observations. Earth Syst. Sci. Data 15 (2), 621–638. https://doi.org/10.5194/essd-15-621-2023.
Joyce, R.J., Janowiak, J.E., Arkin, P.A., Xie, P., 2004. CMORPH: A method that produces global precipitation estimates from passive microwave and infrared data at high spatial and temporal resolution. J. Hydrometeorol. 5 (3), 487–503. https://doi.org/10.1175/1525-7541(2004)005< 0487:CAMTPG> 2.0.CO;2.
Khan, S.I., Hong, Y., Gourley, J.J., Khattak, M.U.K., Yong, B., Vergara, H.J., 2014. Evaluation of three high-resolution satellite precipitation estimates: Potential for monsoon monitoring over Pakistan. Adv. Space Res. 54 (4), 670–684. https://doi.org/10.1016/j.asr.2014.04.017.
Kidd, C., Huffman, G., 2011. Global precipitation measurement. Meteorol. Appli 18 (3), 334–353. https://doi.org/10.1002/met.284.
Kidd, C., Becker, A., Huffman, G.J., Muller, C.L., Joe, P., Skofronick-Jackson, G., Kirschbaum, D.B., 2017. So, how much of the Earth's surface is covered by rain gauges? Bull. Am. Meteorol. Soc. 98, 69–78. https://doi.org/10.1175/bams-d-14-00283.1.
Kumar, S., Amarnath, G., Ghosh, S., Park, E., Baghel, T., Wang, J., Pramanik, M., Belbase, D., 2022. Assessing the performance of the satellite-based precipitation products (SPP) in the data-sparse Himalayan Terrain. Remote Sens 14 (19), 4810. https://doi.org/10.3390/rs14194810.
Lakshmi, V., 2024. Enhancing human resilience against climate change: Assessment of hydroclimatic extremes and sea level rise impacts on the Eastern Shore of Virginia, United States. Sci. Total Environ. 947, 174289. https://doi.org/10.1016/j.scitotenv.2024.174289.
Lakshmi, V., Fayne, J., Bolten, J., 2018. A comparative study of available water in the major river basins of the world. J. Hydrol. 567, 510–532. https://doi.org/10.1016/j.jhydrol.2018.10.038.
Le, M.H., Lakshmi, V., Bolten, J., Du Bui, D., 2020. Adequacy of satellite-derived precipitation estimate for hydrological modeling in Vietnam basins. J. Hydrol. 586, 124820. https://doi.org/10.1016/j.jhydrol.2020.124820.
Le, M.H., Zhang, R., Nguyen, B.Q., Bolten, J.D., Lakshmi, V., 2023. Robustness of gridded precipitation products for Vietnam basins using the comprehensive assessment framework of rainfall. Atmos. Res. 293, 106923. https://doi.org/10.1016/j.atmosres.2023.106923.
Lenderink, G., Buishand, A., Van Deursen, W., 2007. Estimates of future discharges of the river Rhine using two scenario methodologies: direct versus delta approach. Hydrol. Earth Syst. Sci. 11 (3), 1145–1159. https://doi.org/10.5194/hess-11-1145-2007.

Li, R., Shi, J., Ji, D., Zhao, T., Plermkamon, V., Moukomla, S., Kuntiyawichai, K., Kruasilp, J., 2019. Evaluation and hydrological application of TRMM and GPM precipitation products in a tropical monsoon basin of Thailand. Water 11 (4), 818. https://doi.org/10.3390/w11040818.
Li, Z., Yang, D., Hong, Y., 2013. Multi-scale evaluation of high-resolution multi-sensor blended global precipitation products over the Yangtze River. J. Hydrol. 500, 157–169. https://doi.org/10.1016/j.jhydrol.2013.07.023.
Li, Z., Yang, D., Gao, B., Jiao, Y., Hong, Y., Xu, T., 2015. Multiscale hydrologic applications of the latest satellite precipitation products in the Yangtze River Basin using a distributed hydrologic model. J. Hydrometeorol. 16 (1), 407–426. https://doi.org/10.1175/JHM-D-14-0105.1.
Liu, J., Duan, Z., Jiang, J., Zhu, A., 2015. Evaluation of three satellite precipitation products TRMM 3B42, CMORPH, and PERSIANN over a subtropical watershed in China. Adv. Meteor. 2015 (1), 151239. https://doi.org/10.1155/2015/151239.
Luo, M., Liu, T., Meng, F., Duan, Y., Frankl, A., Bao, A., De Maeyer, P., 2018. Comparing bias correction methods used in downscaling precipitation and temperature from regional climate models: a case study from the Kaidu River Basin in Western China. Water 10 (8), 1046. https://doi.org/10.3390/w10081046.
Madsen, H., 1989. Quality control of precipitation measurements in Denmark, in:Proceedings of the fourth International Meeting on Statistical Climatology, Rotura, New Zealand, pp. 13-15.
Maleika, W., 2020. Inverse distance weighting method optimization in the process of digital terrain model creation based on data collected from a multibeam echosounder. Appl. Geomat. 12 (4), 397–407. https://doi.org/10.1007/s12518-020-00307-6.
Mastrantonas, N., Bhattacharya, B., Shibuo, Y., Rasmy, M., Espinoza-Dávalos, G., Solomatine, D., 2019. Evaluating the benefits of merging near-real-time satellite precipitation products: A case study in the Kinu basin region, Japan. J. Hydrometeorol. 20 (6), 1213–1233. https://doi.org/10.1175/JHM-D-18-0190.1.
Mazzoleni, M., Brandimarte, L., Amaranto, A., 2019. Evaluating precipitation datasets for large-scale distributed hydrological modelling. J. Hydrol. 578, 124076. https://doi.org/10.1016/j.jhydrol.2019.124076.
Mehrotra, R., Sharma, A., 2016. A multivariate quantile-matching bias correction approach with auto-and cross-dependence across multiple time scales: Implications for downscaling. J. Clim. 29 (10), 3519–3539. https://doi.org/10.1175/JCLI-D-15-0356.1.
Milford, J.R., McDougall, V.D., Dugdale, G., 1994. Rainfall estimation from cold cloud duration: Experience of the TAMSAT group in West Africa. Validation Problems of Rainfall Estimation by Satellite in Intertropical Africa. ORSTROM, Niamey, Niger, pp. 13–29.
Moges, D.M., Kmoch, A., Uuemaa, E., 2022. Application of satellite and reanalysis precipitation products for hydrological modeling in the data-scarce Porijõgi catchment, Estonia. J. Hydrol.: Reg. Stud. 41, 101070. https://doi.org/10.1016/j.ejrh.2022.101070.
Mondal, A., Lakshmi, V., Hashemi, H., 2018. Intercomparison of trend analysis of multisatellite monthly precipitation products and gauge measurements for river basins of India. J. Hydrol. 565, 779–790. https://doi.org/10.1016/j.jhydrol.2018.08.083.
Moriasi, D.N., Arnold, J.G., Van Liew, M.W., Bingner, R.L., Harmel, R.D., Veith, T.L., 2007. Model evaluation guidelines for systematic quantification of accuracy in watershed simulations. Trans. Asabe. 50 (3), 885–900. https://doi.org/10.13031/2013.23153.
Muhammad, W., Yang, H., Lei, H., Muhammad, A., Yang, D., 2018. Improving the regional applicability of satellite precipitation products by ensemble algorithm. Remote Sens 10 (4), 577. https://doi.org/10.3390/rs10040577.
Mukul, M., Srivastava, V., Mukul, M., 2015. Analysis of the accuracy of Shuttle Radar Topography Mission (SRTM) height models using International Global Navigation Satellite System Service (IGS) Network. J. Earth Syst. Sci. 124, 1343–1357. https://doi.org/10.1007/s12040-015-0597-2.
Nadeem, M.U., Waheed, Z., Ghaffar, A.M., Javaid, M.M., Hamza, A., Ayub, Z., Nawaz, M.A., Waseem, W., Hameed, M.F., Zeeshan, A., 2022. Application of HEC-HMS for flood forecasting in hazara catchment Pakistan, south Asia. Int. J. Hydrol. 6 (1), 7–12. https://doi.org/10.15406/ijh.2022.06.00296.
Neter, J., Kutner, M.H., Nachtsheim, C.J., Wasserman, W., 1996. Appl. Linear Stat. Models.
Nguyen, B.Q., Van Binh, D., Tran, T.N.D., Kantoush, S.A., Sumi, T., 2024. Response of streamflow and sediment variability to cascade dam development and climate change in the Sai Gon Dong Nai River basin. Clim. Dyn. 62 (8), 7997–8017. https://doi.org/10.1007/s00382-024-07319-7.
Nguyen, P., Ombadi, M., Sorooshian, S., Hsu, K., AghaKouchak, A., Braithwaite, D., Ashouri, H., Thorstensen, A.R., 2018. The PERSIANN family of global satellite precipitation data: A review and evaluation of products. Hydrol. Earth Syst. Sci. 22 (11), 5801–5816. https://doi.org/10.5194/hess-22-5801-2018.
Omotosho, T.V., Oluwafemi, C.O., 2009. One-minute rain rate distribution in Nigeria derived from TRMM satellite data. J. Atmos. Sol. -Terr. Phys. 71 (5), 625–633. https://doi.org/10.1016/j.jastp.2009.02.003.
Pakoksung, K., Takagi, M., 2016. Effect of satellite based rainfall products on river basin responses of runoff simulation on flood event. Model. Earth Syst. Environ. 2, 1–14. https://doi.org/10.1007/s40808-016-0200-0.
Pereira, L.S., Paredes, P., Hunsaker, D.J., López-Urrea, R., Shad, Z.M., 2021. Standard single and basal crop coefficients for field crops. Updates and advances to the FAO56 crop water requirements method. Agric. Water Manag. 243, 106466. https://doi.org/10.1016/j.agwat.2020.106466.
Pfeifroth, U., Mueller, R., Ahrens, B., 2013. Evaluation of satellite-based and reanalysis precipitation data in the tropical Pacific. J. Appl. Meteorol. Clim. 52 (3), 634–644. https://doi.org/10.1175/JAMC-D-12-049.1.
Piani, C., Haerter, J.O., Coppola, E., 2010. Statistical bias correction for daily precipitation in regional climate models over Europe. Theor. Appl. Clim. 99, 187–192. https://doi.org/10.1007/s00704-009-0134-9.
Poortinga, A., Bastiaanssen, W., Simons, G., Saah, D., Senay, G., Fenn, M., Bean, B., Kadyszewski, J., 2017. A self-calibrating runoff and streamflow remote sensing model for ungauged basins using open-access earth observation data. Remote Sens 9 (1), 86. https://doi.org/10.3390/rs9010086.
Prakash, S., 2019. Performance assessment of CHIRPS, MSWEP, SM2RAIN-CCI, and TMPA precipitation products across India. J. Hydrol. 571, 50–59. https://doi.org/10.1016/j.jhydrol.2019.01.036.
Prakash, S., Mitra, A.K., AghaKouchak, A., Liu, Z., Norouzi, H., Pai, D.S., 2018. A preliminary assessment of GPM-based multi-satellite precipitation estimates over a monsoon dominated region. J. Hydrol. 556, 865–876. https://doi.org/10.1016/j.jhydrol.2016.01.029.
Rahman, K.U., Shang, S., Shahid, M., Li, J., 2018. Developing an ensemble precipitation algorithm from satellite products and its topographical and seasonal evaluations over Pakistan. Remote Sens 10 (11), 1835. https://doi.org/10.3390/rs10111835.
Rana, S., McGregor, J., Renwick, J., 2015. Precipitation seasonality over the Indian subcontinent: An evaluation of gauge, reanalyses, and satellite retrievals. J. Hydrometeorol. 16 (2), 631–651. https://doi.org/10.1175/JHM-D-14-0106.1.
Rasmy, M., Shrestha, M., Koike, T., Hara, M., Fujita, M., Kimura, F., 2014. A combined dynamical/statistical downscaling approach for assessing future of water resources in the Tone river basin, Japan. 土木学会論文集 B1 (水工学) 70 (4), I_187–I_192. https://doi.org/10.2208/jscejhe.70.I_187.
Ray, R.L., Sishodia, R.P., Tefera, G.W., 2022. Evaluation of gridded precipitation data for hydrologic modeling in North-Central Texas. Remote Sens 14 (16), 3860. https://doi.org/10.3390/rs14163860.
Reek, T., Doty, S.R., Owen, T.W.A., 1992. Deterministic approach to the validation of historical daily temperature and precipitation data from the cooperative network. Bull. Am. Meteorol. Soc. 73 (6), 753–762. https://doi.org/10.1175/1520-0477(1992)073< 0753:ADATTV> 2.0.CO;2.
Sadeghi, M., Nguyen, P., Naeini, M.R., Hsu, K., Braithwaite, D., Sorooshian, S., 2021. PERSIANN-CCS-CDR, a 3-hourly 0.04 global precipitation climate data record for heavy precipitation studies. Sci. Data 8 (1), 157. https://doi.org/10.1038/s41597-021-00940-9.
Saemian, P., Hosseini-Moghari, S.M., Fatehi, I., Shoarinezhad, V., Modiri, E., Tourian, M.J., Tang, Q., Nowak, W., Bárdossy, A., Sneeuw, N., 2021. Comprehensive evaluation of precipitation datasets over Iran. J. Hydrol. 603, 127054. https://doi.org/10.1016/j.jhydrol.2021.127054.
Sharif, R.B., Habib, E.H., ElSaadani, M., 2020. Evaluation of radar-rainfall products over coastal Louisiana. Remote Sens 12 (9), 1477. https://doi.org/10.3390/rs12091477.
Shen, Y., Xiong, A., Wang, Y., Xie, P., 2010. Performance of high-resolution satellite precipitation products over China. J. Geophys. Res.: Atmos. 115 (D2). https://doi.org/10.1029/2009JD012097.
Shepard, D., 1968. A two-dimensional interpolation function for irregularly-spaced data. Proc. 1968 23rd ACM Natl. Conf. 517–524.
Siddig, M.S., Ibrahim, S., Yu, Q., Abdalla, A., Osman, Y., Atiem, I.A., Hamukwaya, S.L., Taha, M.M., 2022. Bias adjustment of four satellite-based rainfall products using ground-based measurements over Sudan. Water 14 (9), 1475. https://doi.org/10.3390/w14091475.
Simons, G., Bastiaanssen, W., Ngo, L.A., Hain, C.R., Anderson, M., Senay, G., 2016. Integrating global satellite-derived data products as a pre-analysis for hydrological modelling studies: a case study for the Red River Basin. Remote Sens 8 (4), 279. https://doi.org/10.3390/rs8040279.

Singh, R., Thakur, D.A., Mohanty, M.P., 2024. Can Satellite Precipitation Products Comprehend Rainfall Extremes Over Disaster-Sensitive Mountainous Basins? An Exhaustive Inter-comparison and Assessment Over Nepal. Earth Syst. Environ. 1–21. https://doi.org/10.1007/s41748-024-00557-z.
Skofronick-Jackson, G., Petersen, W.A., Berg, W., Kidd, C., Stocker, E.F., Kirschbaum, D.B., Kakar, R., Braun, S.A., Huffman, G.J., Iguchi, T., Kirstetter, P.E., 2017. The Global Precipitation Measurement (GPM) mission for science and society. Bull. Am. Meteorol. Soc. 98 (8), 1679–1695. https://doi.org/10.1175/BAMS-D-15-00306.1.
Sorooshian, S., Hsu, K.L., Gao, X., Gupta, H.V., Imam, B., Braithwaite, D., 2000. Evaluation of PERSIANN system satellite-based estimates of tropical rainfall. Bull. Am. Meteorol. Soc. 81 (9), 2035–2046. https://doi.org/10.1175/1520-0477(2000)081< 2035:EOPSSE> 2.3.CO;2.
Sriwongsitanon, N., Kaprom, C., Tantisuvanichkul, K., Prasertthonggorn, N., Suiadee, W., Bastiaanssen, W.G., Williams, J.A., 2023. The combined power of double mass curves and bias correction for the maximisation of the accuracy of an ensemble satellite-based precipitation estimate product. Hydrol 10 (7), 154. https://doi.org/10.3390/hydrology10070154.
Sun, Q., Miao, C., Duan, Q., Ashouri, H., Sorooshian, S., Hsu, K.L., 2018. A review of global precipitation data sets: Data sources, estimation, and intercomparisons. Rev. Geophys 56 (1), 79–107. https://doi.org/10.1002/2017RG000574.
Syed, T.H., Lakshmi, V., Paleologos, E., Lohmann, D., Mitchell, K., Famiglietti, J.S., 2004. Analysis of process controls in land surface hydrological cycle over the continental United States. J. Geophys. Res.: Atmos. 109 (D22). https://doi.org/10.1029/2004JD004640.
Tan, M.L., Duan, Z., 2017. Assessment of GPM and TRMM precipitation products over Singapore. Remote Sens 9 (7), 720. https://doi.org/10.3390/rs9070720.
Tan, M.L., Ibrahim, A.L., Duan, Z., Cracknell, A.P., Chaplot, V., 2015. Evaluation of six high-resolution satellite and ground-based precipitation products over Malaysia. Remote Sens 7 (2), 1504–1528. https://doi.org/10.3390/rs70201504.
Tang, G., Clark, M.P., Papalexiou, S.M., Ma, Z., Hong, Y., 2020b. Have satellite precipitation products improved over last two decades? A comprehensive comparison of GPM IMERG with nine satellite and reanalysis datasets. Remote Sens. Environ. 240, 111697. https://doi.org/10.1016/j.rse.2020.111697.
Tang, G., Clark, M.P., Newman, A.J., Wood, A.W., Papalexiou, S.M., Vionnet, V., Whitfield, P.H., 2020a. SCDNA: A serially complete precipitation and temperature dataset for North America from 1979 to 2018. Earth Syst. Sci. Data 12 (4), 2381–2409. https://doi.org/10.5194/essd-12-2381-2020.
Tapas, M.R., Etheridge, R., Howard, G., Mair, M., 2023. Framework for stakeholder-driven socio-hydrological modeling: conceptual foundations for policy development and evaluation to improve ecosystem health. In: Pandey, M., Umamahesh, N., Das, J., Pu, J.H. (Eds.), Hydrology and Hydrologic Modelling. HYDRO 2023. Lecture Notes in Civil Engineering, 410. Springer, Singapore, pp. 575–589. https://doi.org/10.1007/978-981-97-7474-6_42.
Tapas, M.R., Do, S.K., Etheridge, R., Lakshmi, V., 2024. Investigating the impacts of climate change on hydroclimatic extremes in the Tar-Pamlico River basin, North Carolina. J. Environ. Manag. 363, 121375. https://doi.org/10.1016/j.jenvman.2024.121375.
Taylor, K.E., 2001. Summarizing multiple aspects of model performance in a single diagram. J. Geophys. Res.: Atmos. 106 (D7), 7183–7192. https://doi.org/10.1029/2000JD900719.
Tesfagiorgis, K., Mahani, S.E., Krakauer, N.Y., Khanbilvardi, R., 2011. Bias correction of satellite rainfall estimates using a radar-gauge product–a case study in Oklahoma (USA). Hydrol. Earth Syst. Sci. 15 (8), 2631–2647. https://doi.org/10.5194/hess-15-2631-2011.
Teutschbein, C., Seibert, J., 2013. Is bias correction of regional climate model (RCM) simulations possible for non-stationary conditions? Hydrol. Earth Syst. Sci. 17 (12), 5061–5077. https://doi.org/10.5194/hess-17-5061-2013.
Themeßl, M.J., Gobiet, A., Leuprecht, A., 2011. Empirical-statistical downscaling and error correction of daily precipitation from regional climate models. Int. J. Clim. 31 (10), 1530–1544. https://doi.org/10.1002/joc.2168.
Thom, H.C.S., 1966. Some methods of climatological analysis. in:WMO Technical note, Vol. 81, Secretariat of the World Meteorological Organization: Geneva, Switzerland, p. 53.
Tian, Y., Peters-Lidard, C.D., 2010. A global map of uncertainties in satellite-based precipitation measurements. Geophys. Res. Lett. 37 (24). https://doi.org/10.1029/2010GL046008.
Tong, K., Su, F., Yang, D., Zhang, L., Hao, Z., 2014. Tibetan Plateau precipitation as depicted by gauge observations, reanalyses and satellite retrievals. Int. J. Clim. 34 (2), 265–285. https://doi.org/10.1002/joc.3682.
Tran, T.N.D., Nguyen, B.Q., Zhang, R., Aryal, A., Grodzka-Łukaszewska, M., Sinicyn, G., Lakshmi, V., 2023. Quantification of gridded precipitation products for the streamflow simulation on the Mekong River Basin using rainfall assessment framework: a case study for the Srepok River Subbasin, Central Highland Vietnam. Remote Sens 15 (4), 1030. https://doi.org/10.3390/rs15041030.
Trang, H.T., Manomaiphiboon, K., Singhrattna, N., Assareh, N., 2020. Evaluation of multiple sub-daily satellite precipitation products for Thailand. J. Sustain. Energy Environ. 11, 81–91. ⟨https://www.jseejournal.com/media/236/attachment/Evaluation%20of%20Multiple%20pp.%2081-91.pdf⟩.
Ventura, N.S.L., 2020. Bias correction of satellite precipitation estimates over Thailand. Chulalongkorn Univ. Theses and Diss. (Chula ETD). 157. ⟨https://digital.car.chula.ac.th/chulaetd/157⟩.
Villarini, G., Mandapaka, P.V., Krajewski, W.F., Moore, R.J., 2008. Rainfall and sampling uncertainties: A rain gauge perspective. J. Geophys. Res.: Atmos. 113 (D11). https://doi.org/10.1029/2007JD009214.
Wang, Z., Zhong, R., Lai, C., Chen, J., 2017. Evaluation of the GPM IMERG satellite-based precipitation products and the hydrological utility. Atmos. Res. 196, 151–163. https://doi.org/10.1016/j.atmosres.2017.06.020.
Wen, Y., Schuur, T., Vergara, H., Kuster, C., 2021. Effect of precipitation sampling error on flash flood monitoring and prediction: Anticipating operational rapid-update polarimetric weather radars. J. Hydrometeorol. 22 (7), 1913–1929. https://doi.org/10.1175/JHM-D-19-0286.1.
Willmott, C.J., Matsuura, K., 2005. Advantages of the mean absolute error (MAE) over the root mean square error (RMSE) in assessing average model performance. Clim. Res. 30 (1), 79–82. https://doi.org/10.3354/cr030079.
Xiang, Y., Chen, J., Li, L., Peng, T., Yin, Z., 2021. Evaluation of eight global precipitation datasets in hydrological modeling. Remote Sens 13 (14), 2831. https://doi.org/10.3390/rs13142831.
Xiao, S., Xia, J., Zou, L., 2020. Evaluation of multi-satellite precipitation products and their ability in capturing the characteristics of extreme climate events over the Yangtze River Basin, China. Water 12 (4), 1179. https://doi.org/10.3390/w12041179.
Xie, P., Xiong, A.Y., 2011. A conceptual model for constructing high-resolution gauge-satellite merged precipitation analyses. J. Geophys. Res.: Atmos. 116 (D21). https://doi.org/10.1029/2011JD016118.
Yang, W.T., Fu, S.M., Sun, J.H., Zheng, F., Wei, J., Ma, Z., 2021. Comparative evaluation of the performances of TRMM-3B42 and Climate Prediction Centre Morphing Technique (CMORPH) precipitation estimates over Thailand. J. Meteorol. Soc. Jpn. Ser. Ii. 99 (6), 1525–1546. https://doi.org/10.2151/jmsj.2021-074.
Yang, X., Lu, Y., Tan, M.L., Li, X., Wang, G., He, R., 2020. Nine-year systematic evaluation of the GPM and TRMM precipitation products in the shuaishui river basin in east-central China. Remote Sens 12 (6), 1042. https://doi.org/10.3390/rs12061042.
Yang, Z., Hsu, K., Sorooshian, S., Xu, X., Braithwaite, D., Verbist, K.M., 2016. Bias adjustment of satellite-based precipitation estimation using gauge observations: A case study in Chile. J. Geophys. Res.: Atmos. 121 (8), 3790–3806. https://doi.org/10.1002/2015JD024540.
Yatagai, A., Kamiguchi, K., Arakawa, O., Hamada, A., Yasutomi, N., Kitoh, A., 2012. APHRODITE: Constructing a long-term daily gridded precipitation dataset for Asia based on a dense network of rain gauges. Bull. Am. Meteorol. Soc. 93 (9), 1401–1415. https://doi.org/10.1175/BAMS-D-11-00122.1.
Yong, B., Ren, L.L., Hong, Y., Wang, J.H., Gourley, J.J., Jiang, S.H., Chen, X., Wang, W., 2010. Hydrologic evaluation of Multisatellite Precipitation Analysis standard precipitation products in basins beyond its inclined latitude band: A case study in Laohahe basin, China. Water Resour. Res. 46 (7). https://doi.org/10.1029/2009WR008965.
Yu, L., Zhang, Y., Yang, Y., 2020. Using high-density rain gauges to validate the accuracy of satellite precipitation products over complex terrains. Atmos 11 (6), 633. https://doi.org/10.3390/atmos11060633.
Yuan, F., Zhang, L., Win, K.W.W., Ren, L., Zhao, C., Zhu, Y., Jiang, S., Liu, Y., 2017. Assessment of GPM and TRMM multi-satellite precipitation products in streamflow simulations in a data-sparse mountainous watershed in Myanmar. Remote Sens 9 (3), 302. https://doi.org/10.3390/rs9030302.

Yuan, F., Wang, B., Shi, C., Cui, W., Zhao, C., Liu, Y., Ren, L., Zhang, L., Zhu, Y., Chen, T., Jiang, S., 2018. Evaluation of hydrological utility of IMERG Final run V05 and TMPA 3B42V7 satellite precipitation products in the Yellow River source region, China. J. Hydrol. 567, 696–711. https://doi.org/10.1016/j.jhydrol.2018.06.045.

Zhou, L., Koike, T., Takeuchi, K., Rasmy, M., Onuma, K., Ito, H., Selvarajah, H., Liu, L., Li, X., Ao, T., 2022. A study on availability of ground observations and its impacts on bias correction of satellite precipitation products and hydrologic simulation efficiency. J. Hydrol. 610, 127595. https://doi.org/10.1016/j.jhydrol.2022.127595.

Zhu, Q., Luo, Y., Zhou, D., Xu, Y.P., Wang, G., Gao, H., 2019. Drought monitoring utility using satellite-based precipitation products over the Xiang River Basin in China. Remote Sens 11 (12), 1483. https://doi.org/10.3390/rs11121483.